

Aus dem Institut für Anatomie

Direktor: Uni. Prof. Dr. med. Dr. rer. nat. Markus Kipp

Astrocytic expression of  
aldehyde dehydrogenase family 1 member L1

Dissertation

Erlangung des akademischen Grades an der  
Doktor der Medizin (Dr. med.)  
der Universitätsmedizin Rostock

vorgelegt von

Feifei Liu

23.09.1985, Henan, China

Rostock, 2022

Reviewer:

1. Reviewer: Prof. Dr. med. Dr. rer. nat. Markus Kipp, Institut für Neuroanatomie,  
Universitätsmedizin Rostock

2. Reviewer: Prof. Dr. med. Andreas Büttner, Institut für Rechtsmedizin,  
Universitätsmedizin Rostock

3. Reviewer: PD Dr. rer. nat. Tim Clamer, Institut für Neuroanatomie,  
Universitätsklinikum Aachen

Date of submission: 24.10.2022

Date of defense: 22.02.2023

# Table of contents

1. Abstract.....	5
2. Abbreviations .....	6
3. Introduction .....	8
3.1 MS .....	8
3.1.1 Etiology .....	8
3.1.2 Pathology.....	9
3.1.3 Symptoms.....	9
3.1.4 Clinical phenotypes .....	9
3.1.5 Pathogenesis .....	10
3.2 Animal models of MS.....	11
3.2.1 Experimental autoimmune encephalomyelitis models .....	11
3.2.2 Cuprizone intoxication model .....	12
3.3 Astrocyte .....	13
3.3.1 The function, physiology, and pathology of astrocytes.....	14
3.3.2 Heterogeneity of Astrocytes.....	17
3.3.3 Markers of astrocyte .....	17
3.4 Aim of this study.....	18
4. Materials and methods .....	20
4.1 Animals .....	20
4.2 Transcardial perfusion and tissue processing .....	21
4.3 Human brain tissues .....	22
4.4 Immunohistochemistry.....	23
4.4.1 Principle of immunohistochemical staining.....	23
4.4.2 Procedure of Immunohistochemical staining.....	24
4.5 Immunofluorescence .....	28
4.5.1 Principle of immunofluorescent staining .....	28
4.5.2 Procedure of double immunofluorescent staining .....	30
4.6 Negative controls .....	32
4.7 Digital Image Analysis .....	33
4.7.1 Quantification of single cellular area.....	33
4.7.2 Quantification of staining intensity .....	34
4.7.3 ROIs.....	36
4.7.4 Quantification of cell density .....	37
4.8 Statistical Analysis .....	37
5. Results.....	38

5.1 Protoplasmic and fibrous pattern .....	38
5.2 ALDH1L1 expression in human cortex .....	39
5.3 GFAP expression in human cortex .....	41
5.4 ALDH1L1 expression in murine cortex .....	42
5.5 Cellular areas of astrocytes .....	43
5.6 Relations between astrocytes with low ALDH1L1 expression and blood vessels.....	47
5.7 ALDH1L1 expression in post-mortem MS tissues .....	48
5.8 Astrocytic ALDH1L1 expression in cuprizone models .....	50
5.9 Negative controls .....	51
6. Discussion .....	53
6.1 The expression of ALDH1L1 by astrocytes .....	53
6.2 Other markers of astrocytes .....	54
6.3 Astrocyte response and function in MS .....	55
6.4 The function of ALDH1L1 in CNS. ....	59
7. Conclusion .....	61
8. List of figures .....	62
9. List of tables.....	63
10. References .....	64
11. Appendix .....	77
11.1 Chemicals .....	77
11.2 Solutions .....	78
12. Personal declaration .....	79
13. Acknowledgements.....	80
14. Curriculum Vitae .....	81

# 1. Abstract

Astrocytes are the most numerous cell population of glia in the central nervous system (CNS). With ubiquitous distribution in the CNS and complex interactions with other elements of neural circuits, astrocytes exert diverse and vital functions. Astrocytes maintain the integrity of the blood-brain barrier (BBB), provide trophic support to neurons, modulate synapse formation, recycle neurotransmitters, maintain ion and water homeostasis, and actively interact with other glial cells. In addition, astrocytes respond to all kinds of CNS insults, through a process referred to as “reactive astrogliosis”. This study mainly focused on the astrocytic expression of aldehyde dehydrogenase family 1 member L1 (ALDH1L1) under physiological and pathological conditions. To this end, brain sections from 3 control humans, 3 multiple sclerosis (MS) patients, 5 control mice, and 15 mice intoxicated with cuprizone were applied. Immunohistochemical and immunofluorescent staining was performed to analyze the expression of ALDH1L1 by astrocytes. The results indicated that a proportion of cortical astrocytes reduced the expression of ALDH1L1 in a region-dependent manner; in MS, the expression of ALDH1L1 by some astrocytes seemed centralized to the somas of astrocytes; in the cuprizone model, significant astrogliosis in the medial part of the corpus callosum was found by immunohistochemistry. In summary, these data suggest a dynamic regulation of ALDH1L1 in both the healthy and diseased CNS.

## 2. Abbreviations

ABC: avidin-biotin complex

ALDH1L1: aldehyde dehydrogenase family 1 member L1

AQP4: aquaporin-4

BBB: blood-brain barrier

CCL: C-C motif chemokine ligand

CD: cluster of differentiation

CNS: central nervous system

CSF: cerebrospinal fluid

Cup: Cuprizone

Cx43: connexin-43

CXCL: C-X-C Motif chemokine Ligand

CXCR: C-X-C Motif chemokine Receptor

DAB: 3,3'-Diaminobenzidine

DAPI: 4',6-diamidino-2-phenylindole

EAE: experimental autoimmune encephalomyelitis

EBV: Epstein-Barr virus

EDTA: ethylenediaminetetraacetic acid

GFAP: glial fibrillary acidic protein

GLT1: glutamate transporter-1

GM-CSF: granulocyte-macrophage colony-stimulating factor

HCl: hydrogen chloride

HIER: heat induced antigen retrieval

HLA: human leukocyte antigen

HRP: horseradish peroxidase

IL: interleukin

KCl: potassium chloride

KH<sub>2</sub>PO<sub>4</sub>: potassium dihydrogen phosphate  
LPS: Lipopolysaccharide  
MBP: myelin basic protein  
MHC: major histocompatibility  
MOG: oligodendrocyte glycoprotein  
MRI: magnetic resonance imaging  
mRNA: messenger ribonucleic acid  
MS: multiple sclerosis  
Na<sub>2</sub>HPO<sub>4</sub>: disodium hydrogen phosphate  
NaH<sub>2</sub>PO<sub>4</sub>: sodium dihydrogen phosphate  
NaCl: sodium chloride  
NaOH: sodium hydroxide  
OPCs: oligodendrocyte progenitor cells  
PBS: phosphate-buffered saline  
PLP: proteolipid proteins  
ROI: region of interest  
PPMS: primary progressive multiple sclerosis  
RRID: research resource identifier  
RRMS: relapsing-remitting multiple sclerosis  
SEM: standard error of the mean  
SPMS: secondary progressive multiple sclerosis  
TNF: tumor necrosis factor  
Th: T helper

# 3. Introduction

## 3.1 MS

MS is generally thought to be a chronic inflammatory disease mainly affecting the CNS, causing sensory, motor, and cognitive function disorders.

### 3.1.1 Etiology

About 2.8 million people suffer from MS all over the world [1]. MS mainly occurs in adults and is one of the common diseases resulting in disability in adults between 15 and 60 years old. Data show that compared with males, females are more susceptible to MS, with a ratio of about 1:2.3-3.5 [2].

Although significant advances in understanding the MS pathology have been made, the exact cause remains uncertain, and currently, multiple factors have been shown to be related to the development of MS. Latitudes gradient is identified as an essential factor influencing the incidence of MS, implying the environmental effect on the development of MS [3]. Because individuals living in high latitudes usually get less sunlight exposure, they thus generate less vitamin D in response, and these two factors have been linked to MS prevalence [4,5].

Viral infections have been proposed as another risk factor in the development of MS, especially Epstein–Barr virus (EBV). EBV infection could increase the risk of MS onset by 32-fold [6]. It has been demonstrated that antibodies to EBV cross-react with GlialCAM, a glial cell adhesion molecule [7], in addition, exposure to EBV induces myelin-reactive autoantibodies in vivo in mice [8].

For decades, attention has been focused on potential genetic components associated with MS. One example that could prove the association is the concordance rate of MS in monozygotic twins can reach up to 25%, and in contrast, it is only 3% in dizygotic twins [9], both of which are much higher than the incidence of 0.2% in the general population. One more example is the prevalence of MS in some ethnic groups is lower,



making it seem that these groups are born with a kind of resistance, e.g., in some Asian [10] and Middle East countries [11]. In recent years, studies have revealed that apart from human leukocyte antigen (HLA) class II alleles [12] which have been identified in some MS cases, more than 110 genetic variants [13] could increase the individual susceptibility to MS. Most of these genes are related to the immune system.

### **3.1.2 Pathology**

The pathological features of MS include multiple aspects, e.g., demyelinated lesions, oligodendrocyte apoptosis, axonal loss, infiltrating immune cells, microglia activation, and reactive astrogliosis [14].

Demyelinated lesions can be found in all parts of the CNS, including white matter and grey matter in the cortex, cerebellar, brain stem, and spinal cord [15].

### **3.1.3 Symptoms**

A variety of clinical manifestations corresponding to the function of the regions affected are present in MS patients. The common symptoms include vision loss, diplopia, limb sensory disorders, limb movement disorders, ataxia, and bladder or rectal dysfunction [16]. Individuals usually exhibit one symptom or a combination of several symptoms.

### **3.1.4 Clinical phenotypes**

According to the disease course characteristics, there are three common clinical phenotypes.

Relapsing-remitting multiple sclerosis (RRMS): The majority of MS patients (about 85%) initially suffer from discrete episodes of neurological symptoms (i.e. relapsing), followed by partial or complete function recovery (i.e. remitting) [17].

Secondary progressive multiple sclerosis (SPMS): More than 50% of patients with RRMS step into a continuous worsening period without relapses and remissions. The transition usually happens 10-15 years after disease onset [18].

Primary progressive multiple sclerosis (PPMS): About 10% of all MS patients exhibit a

slowly progressive exacerbation without remission from disease onset [19].

In addition, there are other less common forms of MS with distinct disease courses.

Benign MS refers to a small proportion of MS patients who experience a relatively stable situation with mild neurological symptoms or without symptoms and attacks within 15 years after disease onset [20].

Malignant MS starts with an attack and reaches its peak rapidly within a short period of time, resulting in severe neurological deficits or even death [21].

### 3.1.5 Pathogenesis

The pathogenesis of MS remains elusive. Currently, there are two complementary hypotheses in debate, “outside-in” and “inside-out”.

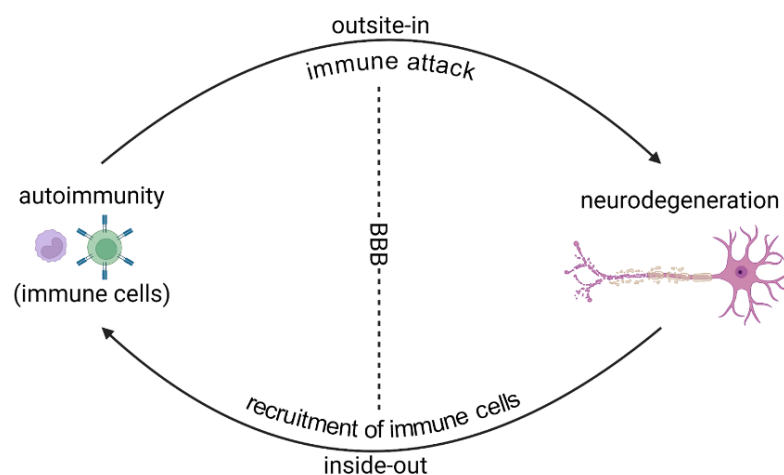


Figure 1: Schematic of MS pathogenesis hypothesis.

The “outside-in” paradigm proposes that activated peripheral immune cells migrate into the CNS and initiate immune attacks on myelin and axons, leading to demyelination and neurodegeneration. The “inside-out” paradigm suggests that primary neurodegenerative events trigger the recruitment of peripheral immune cells into CNS and subsequent inflammation develops, leading to demyelination and further neurodegeneration.

The outside-in paradigm refers to a mechanism that activated peripheral immune cells pass the BBB and damage the CNS components such as oligodendrocytes, causing autoimmune activity and neurodegeneration consequently. Briefly, neurodegeneration is the result of the primary autoimmune process [22,23].

Others support the inside-out hypothesis which states that primary neurodegeneration in situ effectively triggers the immune system, leading to the recruitment of peripheral immune cells into CNS and a subsequent autoimmune attack. In short, primary neurodegeneration is at the root of autoimmune inflammation [22,23].

## **3.2 Animal models of MS**

To recapitulate the various but distinct pathological processes of MS, several animal models have been developed for their application during preclinical studies. It should be noted that these animal models only partially reproduce the various and complex pathological aspects of MS. In addition, there are still some limitations of these animal models because they fail to reflect the temporal and spatial complexity of MS pathology.

### **3.2.1 Experimental autoimmune encephalomyelitis models**

Experimental autoimmune encephalomyelitis (EAE), an immune-mediated animal model mimicking the outside-in paradigm of MS, can be induced in rats [24], zebrafish [25], guinea pigs [26], rabbits [27], primates [28], and most commonly, mice [29]. To induce EAE models in mice, several methods have been established. They can be categorized into three types: sensitization with CNS antigen [30], adoptive transfer of auto-reactive T cells [31], and gene-modified mice with auto-reactive T cell receptors [32].

To sensitize animals, several CNS antigens have been applied, such as spinal cord homogenate [33], various myelin related proteins, including myelin oligodendrocyte glycoprotein (MOG) [34], myelin basic protein (MBP) [35], and proteolipid proteins (PLP) [36].

Different combinations of antigens and mice of genetic backgrounds could induce various disease courses. For example, C57BL/6 mice immunized with MOG35–55 emulsified in complete Freund's adjuvant enriched with Mycobacterium Tuberculosis and with the supplement of pertussis toxin exhibit monophasic disease course [34].

SJL/J mice sensitized with PLP139-151 present with a RRMS like disease course [37]. After EAE induction, about 80% of mice exhibit neurological symptoms in an ascending way, initially tail movement disorder, afterwards hind limb paralysis, then forelimb paralysis [30,38]. In agreement with these ascending symptoms, a study revealed the increase in autoreactive T-cells in the 5th lumbar cord at the early stage of EAE by T2-weighted signals of ultrahigh-field magnetic resonance imaging (MRI) [39].

Sensitized EAE models have an advantage because they allow for analyzing the distinct functions of the respective genes and molecules when established with transgenic mice. Nevertheless, in this model, the inflammatory process is predominately mediated by cluster of differentiation (CD) 4<sup>+</sup> T-cells [40], which is different from MS where the lesions are predominantly infiltrated by CD8<sup>+</sup> T-cells [41]. Meanwhile, in this animal model, lesions can be found frequently in the spinal cords, especially the lumbar spinal cords [39], less frequently in the brain stem and cerebellum, and seldom in the forebrain. In contrast, MS could affect nearly all the parts of the CNS. The predilection sites of lesions in MS are optic nerves, juxtacortical white matter, periventricular region, cerebellum, and cervical spinal cords [42].

### **3.2.2 Cuprizone intoxication model**

In recent decades, the cuprizone intoxication model, which is characterized by demyelinated lesions in the CNS through metabolism abnormalities independent of autoimmune components, has become popular due to its unique mechanism mimicking the inside-out paradigm of MS.

Cuprizone, a neurotoxic copper chelator, when supplemented into standard rodent chow, induces primary oligodendrocytes apoptosis and secondary demyelination in mice. After cuprizone intoxication termination, spontaneous remyelination occurs. Consequently, the cuprizone model offers a platform to investigate the demyelination and/or remyelination process as well as potential molecular changes related to these pathologies.

The dose of the cuprizone is an important factor that affects the pathology in this model.

In order to establish the cuprizone intoxication model in C57BL/6 mice, the appropriate dose of cuprizone is 0.2%-0.3%, because extensive demyelination in the corpus callosum is not stably induced when 0.1% cuprizone is applied, and severe weight loss and high mortality may be caused by cuprizone intoxication of higher dose (0.3%–0.5%) [43]. Apart from the dose of cuprizone, several factors such as gender [44], age [45], mouse strain [46], and the exposure time to cuprizone intoxication [47] have an influence on the demyelination and/or remyelination process. A study reported that extensive demyelination was detected in the corpus callosum and the cortex of C57BL/6 mice after cuprizone intoxication for six weeks, efficient remyelination in the corpus callosum and cortex was confirmed when the cuprizone intoxication was terminated. When the cuprizone intoxication was prolonged to 12 weeks, in this case of chronic demyelination, the endogenous remyelination capacity was impaired [48]. Primary oligodendrocyte apoptosis, secondary demyelination, astrogliosis, and activation of microglia are hallmarks of the cuprizone-induced pathology. Although some authors stated that in this model, the BBB remained intact [43] without T cells infiltration [44], a recent study revealed that BBB had been impaired before demyelination [45]. Our group revealed that CD8<sup>+</sup> T cells were remarkably recruited to cuprizone-induced demyelinated lesions [46]. Besides the corpus callosum was established as a region of interest due to nearly complete demyelination [47], gray matter, including the cortex, the nucleus subthalamicus, the zona incerta, the substantia innominata, the globus pallidus, and the lateral parts of the caudoputamen exhibited severe demyelination as well [48].

### **3.3 Astrocyte**

Astrocytes are essential players in the pathology of MS and its animal models. In recent decades, more and more interest has been aroused in the research into astrocytes and their function in MS.

### 3.3.1 The function, physiology, and pathology of astrocytes

Together with oligodendrocytes, microglia, and ependymal cells, astrocytes constitute glia cells in the CNS. With ubiquitous distribution in the CNS and complex interactions with other elements of neural circuits, the versatile astrocytes exert diverse and vital functions.

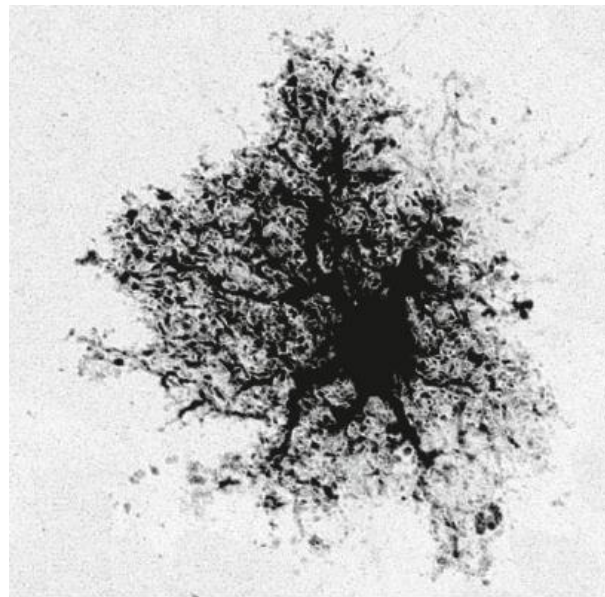


Figure 2: Image of a single protoplasmic astrocyte.

A single protoplasmic astrocyte in the cortex is visualized by injection of a fluorescent dye. The dark round soma is in the center and sprouts out stem processes which give rise to large amounts of finely branched tiny processes (image from [49]).

With a variety of end-feet surrounding blood vessels, astrocytes not only take part in maintaining the BBB but also work as a bridge to transport molecules and metabolites between vasculatures and other elements in the CNS. They provide trophic support to neurons [50], modulate synapse formation [51], recycle neurotransmitters [52], and maintain ion and water homeostasis [53,54].

Gap junctions between astrocytes enable astrocytes to form a functionally coupled network as a syncytium [55]. At the same time, astrocytes have intimate interactions with other glial cells through gap junctions and molecule secretion.

Astrocytes have close communications with microglia. Neurotoxic astrocytes could be

induced after mice were injected with Lipopolysaccharide (LPS), and these neurotoxic astrocytes are referred to as A1 phenotype [56]. In the same study it was shown that interleukin (IL)-1 $\alpha$ , tumor necrosis factor (TNF)- $\alpha$ , and complement component 1q secreted by activated microglia could induce the neurotoxic reactive astrocyte phenotype [56]. Vice versa, astrocytes may induce microglial activation by producing granulocyte-macrophage colony-stimulating factor (GM-CSF), a regulator of microglial activation [57].

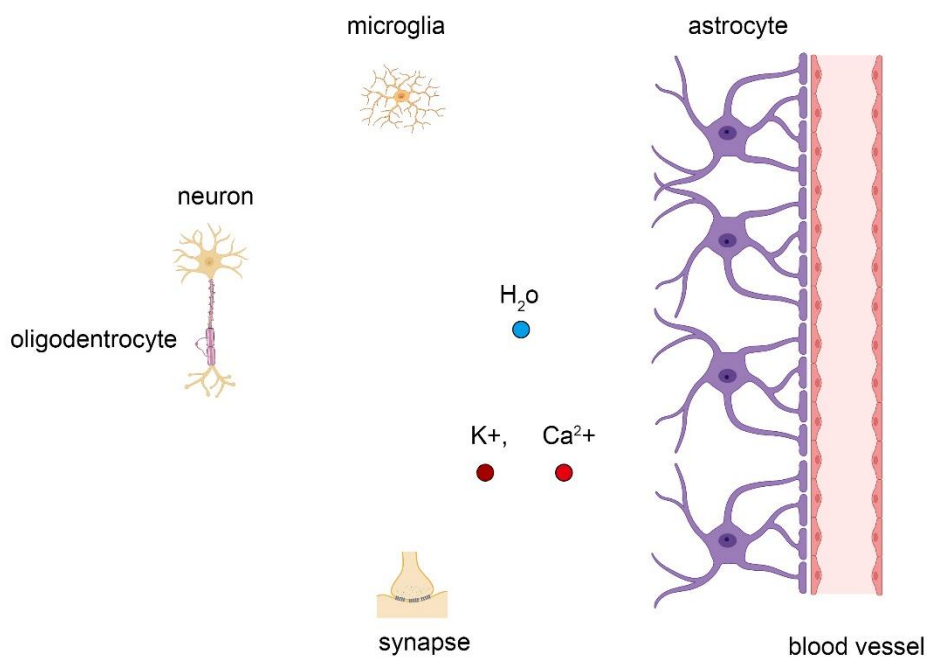


Figure 3: Schematic of complex function of astrocytes.

Astrocytes take part in the constitution of BBB, have close communications with neurons, oligodendrocytes, and microglia, regulate the formation of synapses, maintain the homeostasis of fluid, ions, and transmitters.

Astrocytes have an intimate and close crosstalk to oligodendrocytes. On the one hand, astrocytes facilitate the survival, differentiation, maturation of oligodendrocytes, and the proliferation of oligodendrocyte progenitor cells (OPCs). On the other hand, several molecules secreted by astrocytes, e.g. endothelin-1, could hinder the proliferation and differentiation of OPCs [58]. In return, OPCs could affect the astrocyte foot processes and vascular permeability in MS [59]. And some molecules, e.g., GM-CSF, are

expressed by both astrocytes and oligodendrocytes, indicating the close relations between them.

Astrocytes are implicated in the pathology of all kinds of CNS insults, including MS. As shown in figure 4, under physiological condition, only a proportion of astrocytes express glial fibrillary acidic protein (GFAP). After being triggered by CNS injuries or diseases, astrocytes exhibit morphological changes, molecular and functional alterations. An increased number of astrocytes express GFAP, and stem processes of some astrocytes become hypertrophic. Under severe conditions, astrocytes proliferate and predominantly contribute to glial scar formation. All these changes together are referred to as “reactive astrogliosis”, “reactive astrocytosis”, or “astrocyte activation” [60].



Figure 4: Schematic of astrogliosis.

Under physiological condition, not all astrocytes are GFAP positive. In mild to moderate astrogliosis, more astrocytes are GFAP+, and some astrocytes exhibit a hypertrophic morphology. In severe cases, astrocytes proliferate and contribute to the formation of glial scar.

It has been shown that, in the context of different triggering events, reactive astrocytes exhibit different phenotypes with different properties. Apart from the aforementioned A1 phenotype, the A2 phenotype promoting neural protection was identified in an animal model of cerebral ischemia through cerebral artery occlusion [56]. There are some advocations that the dichotomy is inappropriate because astrocytes could possess both proinflammatory and protective factors at the very same time.



### **3.3.2 Heterogeneity of Astrocytes**

At the same time, morphological heterogeneity and subtype diversity of astrocytes have been studied. Initially, protoplasmic and fibrous astrocytes were identified in the gray matter and white matter, respectively. In the CNS of individuals of higher evolution level, astrocytes tend to exhibit more complex morphology and more diverse subtypes. Interlaminar and varicose projection astrocytes were found to exist mainly in the primate cerebral cortex [61–64]. In the cerebrum, Bergmann glial cells around Purkinje neurons have similar functions as astrocytes in the cortex. Consequently, Bergmann glial cells are usually seen as a subpopulation of astrocytes [65]. Likewise, pituicytes in the pituitary gland are also taken as specialized astrocytes [66]. Currently, it has been confirmed that astrocytes consist of at least nine subpopulations [67].

Considering the heterogeneous subpopulations and complex function in the physiology and pathology of CNS and the aroused interest in investigation into astrocytes, it is of great importance to find an appropriate astrocytic marker and study its expression characteristics in experimental models and diseases.

### **3.3.3 Markers of astrocyte**

Several antibodies have been used to label astrocytes, including GFAP, S100 calcium-binding protein $\beta$  (S100 $\beta$ ), glutamate transporter-1 (GLT1), aquaporin-4 (AQP4), connexin-43 (Cx43), and recently, ALDH1L1 [68].

The most commonly used marker of astrocyte is GFAP, yet GFAP has some properties that one should be aware of. Firstly, GFAP mainly labels somas and stem processes of astrocytes, which misses the details of extensive finely branched processes and consequently does not reflect the real astrocytic morphology and their complete cellular territory [69]. In addition, astrocytes in the white matter can be well visualized by GFAP, while in the gray matter, only astrocytes near the glia limitans superficialis and perivascularis express GFAP in the healthy brain; the remaining astrocytes in the cortex are likely to be GFAP negative, at least during physiological conditions.

Moreover, neural progenitor cells generating astrocytes, neurons, and oligodendrocytes could express GFAP at some time point [70]. Beyond, when astrogliosis initiates, the expression of GFAP is up-regulated, and more astrocytes express GFAP at the cellular level.

ALDH1L1 has been proven to be a specific pan-astrocyte marker, which labels the finely branched processes and, thus, better reflects the real morphology of astrocytes compared with GFAP [68]. Zamanian and her colleagues pointed out that the expression level of ALDH1L1 stayed comparable in purified astrocytes from healthy and injured brains [71]. In contrast, Yang and her colleagues concluded that reactive astrocytes up-regulated ALDH1L1 expression under pathological conditions [72]. Moreover, it was reported that postnatal neural stem cells express ALDH1L1 as well in the brain [73].

### **3.4 Aim of this study**

During initial studies when I applied the anti-ALDH1L1 antibodies to label astrocytes, I found some weakly stained areas as exemplarily demonstrated in figure 5. At the center of such weakly stained areas, somas and stem processes were labeled by the anti-ALDH1L1 antibodies. Based on these observations, I assumed that these cells with low anti-ALDH1L1 staining intensity were astrocytes which, in contrast to most other astrocytes, do not express ALDH1L1 at the fine peripheral processes but just around the perinuclear compartment. The results seemed that these weakly stained astrocytes downregulated the expression of ALDH1L1 in their peripheral regions at the cellular level. To our knowledge, the astrocytic expression loss of ALDH1L1 has not been mentioned yet.

In this study, I therefore addressed the following three hypotheses:

- ◆ These cells with weak ALDH1L1 expression in the cortex are indeed astrocytes.
- ◆ The expression loss of ALDH1L1 happens in a region-dependent manner.
- ◆ ALDH1L1 is competent as a marker of astrocytes.

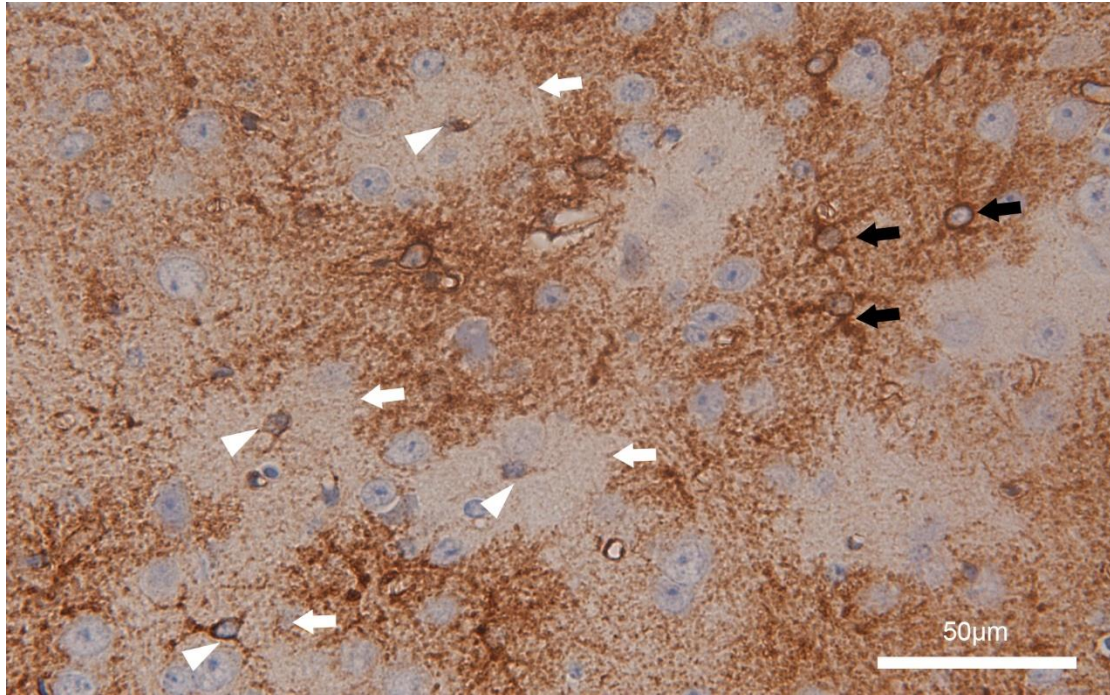


Figure 5: Schematic of astrocytes with weak anti-ALDH1L1 staining intensity.

In the rodent cortex, some astrocytes were visualized by anti-ALDH1L1 immunohistochemical staining and displayed normal staining intensity (black arrows). There were some weakly stained areas in the cortex as well. In the center of the weakly stained areas (white arrows), somas and stem processes (white arrowheads) were labeled by the anti-ALDH1L1 antibodies, and nuclei were visualized by counterstain, indicating these cells with weak staining intensity might be astrocytes.

## 4. Materials and methods

### 4.1 Animals

10-week-old female mice of C57BL/6J strain purchased from Janvier Labs (Le Genest-Saint-Isle, France) were included in this study. Animals were maintained under the standard condition in accordance with the guidelines and recommendations released by the Federation of European Laboratory Animal Science Association (FELASA). No more than five animals were housed in each cage (500 cm<sup>2</sup>). Cages, straws, and nestlets were changed 3 times every week. Animals were maintained in the environment of 12 h light/dark cycle, with temperature controlled between 23 °C ± 2 °C and humidity controlled between 50% ± 5%. Food and water were supplied ad libitum. Prior to the initiation of the experiments, mice were allowed to adapt to the environment for at least 1 week. Body weights of mice were weighed and documented once each week. Health monitoring of the animals was performed daily during the experiment. This animal experiment was approved by the review board for care of animal subjects of the district government with the number 7221.3.1-001/19.

In this study, 20 mice were randomly divided into four groups: (A) control group, standard rodent chow was provided to the animals in this group throughout the whole procedure of the study; (B) 1-week cuprizone group, (C) 3-week cuprizone group, (D) 5-week cuprizone group. Each group consisted of 5 mice. Animals of cuprizone groups were fed with toxic copper chelator cuprizone (Sigma-Aldrich, Taufkirchen, Germany) mixed into standard rodent chow. The toxic chow was prepared freshly every day. Standard rodent chow and cuprizone were weighed by an electronic precision scale and mixed thoroughly by a food processor (Kult X, WMF, Geislingen, Germany). Cuprizone intoxication was supplied to B group for 1 week, C group for 3 weeks, and D group for 5 weeks, respectively. Tissue processing of control group was at the end of 5 weeks, and tissue processing of each cuprizone intoxication group was performed at the end of the cuprizone intoxication (1 week, 3 weeks, or 5 weeks).

In case that animals suffered from a poor physical condition, strict exclusion criteria were applied. Significant weight loss (> 10% within 24 h), severe behavioral deficits (decreased movement, seizure, coma), and infections were considered as exclusion criteria. None of the animals met the exclusion criteria throughout the experiment.

## 4.2 Transcardial perfusion and tissue processing

At first, narcosis of mice was induced through intraperitoneal injection of mixed agents of ketamine (100 mg/kg) and xylazine (10 mg/kg).

Table 1: Preparation of perfusion solution

Step	Process
1	Calculate the desired total solution volume and dosing of ingredients. For 1 liter of 3.7% perfusion solution, 4.6g sodium dihydrogen phosphate ( $\text{NaH}_2\text{PO}_4$ ), 8.0g disodium hydrogen phosphate ( $\text{Na}_2\text{HPO}_4$ ), and 100ml 37% formaldehyde solution should be added.
2	Dissolve $\text{NaH}_2\text{PO}_4$ and $\text{Na}_2\text{HPO}_4$ in distilled water (80% of the total solution volume).
3	Add 37% formaldehyde solution.
4	Stir the solution to mix all the components evenly and set the pH value of the solution to 7.4 by adding dropwise sodium hydroxide (NaOH) or hydrogen chloride (HCL).
5	Fill up the solution to desired volume with distilled water.
6	Filter the solution and store it at 4°C.

After toe-pinch reflex and corneal reflex turned negative, the skin and peritoneum in lower abdomen were cut open to the diaphragm. Afterwards, the diaphragm was dissected, and the ventral thoracical wall (i.e. sternum and ribs) was removed to reveal the entire heart. A small incision was made in the right atrium of the heart, then a blunt syringe needle was punctured into the left ventricle, next, each animal was transcardially perfused with 20 ml of ice-cold phosphate-buffered saline (PBS) followed by 30 ml of perfusion solution (Table 1). After that, perfusion proceeded for another 7 minutes with perfusion solution using an electronic pump (IsmaTec, IPC-4) at a rate of about 22ml/min. Then the head was cut off, and the cranial calvaria was partially removed along the midline. Then the entire head was immersed in 3.7% formaldehyde

solution overnight at 4°C.

The next day, the brain tissues were dissected and placed into tissue cassettes. These brain tissue cassettes were washed with running tap water for 6-12 hours and incubated in 50% ethanol at 4°C overnight. These tissues cassettes were transferred into Histokinette, a dehydration processor in which dehydration of tissues was processed step by step automatically (Table 2). Then, brain tissues were embedded in melted paraffin. Later, the paraffin blocks were placed on the cooling plate overnight to solidify the paraffin.

Subsequently, 5- $\mu$ m-thick coronal sections were sliced using a rotary microtome (RM2255, Leica Microsystems, Wetzlar, Germany) at the level of 285 according to the mouse brain atlas published by Sidman et al. [74]. The paraffin sections were flattened in a warm water bath at 45 °C. Each section or two sections was transferred onto one microscope slide and dried overnight at 37°C in a heating incubator.

Table 2: Tissue dehydration in Histokinette

Step	Duration
70% ethanol	40 minutes
70% ethanol	40 minutes
96% ethanol	40 minutes
96% ethanol	40 minutes
100% ethanol	40 minutes
100% ethanol	40 minutes
100% ethanol	60 minutes
Xylene	40 minutes
Xylene	40 minutes
Xylene	40 minutes
Paraffin (65°C)	60 minutes
Paraffin (65°C)	60 minutes
Paraffin (65°C )	2 days

### 4.3 Human brain tissues

Paraffin-embedded control human brain tissues were obtained according to a rapid autopsy protocol from body donors in Rostock. Paraffin-embedded post-mortem MS

brain tissues were obtained according to a fast autopsy protocol from donors with progressive MS, in collaboration with the Netherlands Brain Bank in Amsterdam. All donors or their relatives had signed an informed consent form for the application of their brain tissues for research. Brain tissues from 3 control donors and 3 donors with MS processed by another MD student from our laboratory (Hannes Kaddatz) were included in this study.

## **4.4 Immunohistochemistry**

### **4.4.1 Principle of immunohistochemical staining**

The immunohistochemistry staining with avidin-biotin complex (ABC) method is a technique that is used for identifying antigens or proteins in situ in tissue sections. The main principle is based on specific immunoreaction as follows:

- ◆ Primary antibody binds specifically to the targeting antigen in biological tissues.
- ◆ Biotin conjugated secondary antibody binds specifically to the primary antibody.
- ◆ The avidin-biotin complex coupled with horseradish peroxidase (HRP) binds to the biotin-conjugated secondary antibody. Biotin–avidin binding is a rapid and one of the most robust natural noncovalent interactions. At the same time, the ABC-HRP system helps amplify the antigen signal.
- ◆ 3,3'-Diaminobenzidine (DAB), a chromogen applied in immunohistochemical staining, is oxidized, and forms a brown precipitate which can be observed under the light microscopy. The oxidative reaction is catalyzed by hydrogen peroxide induced by HRP.

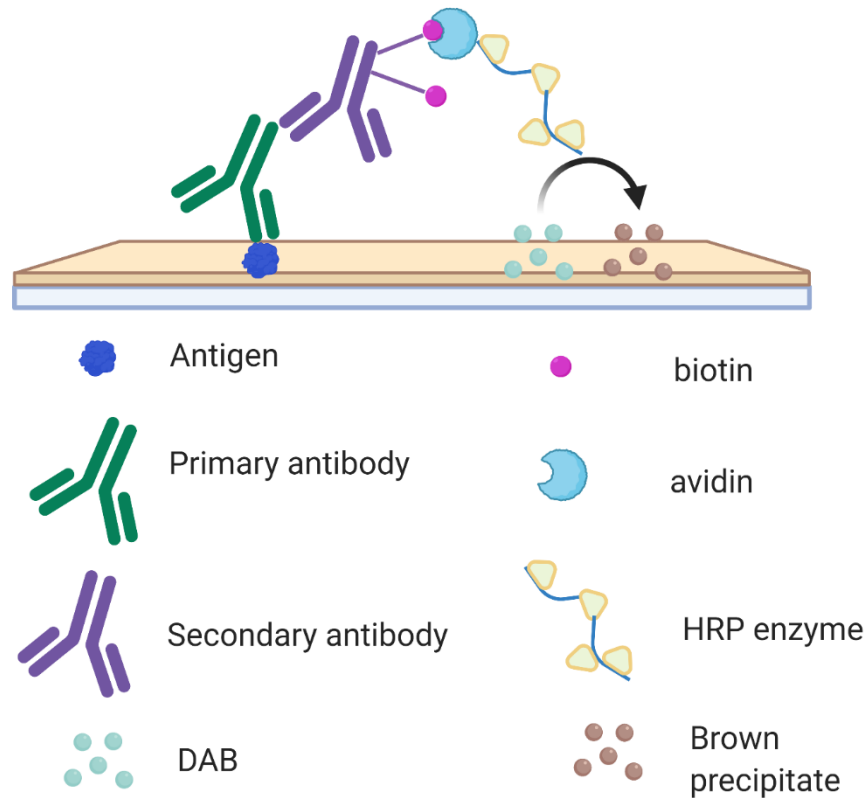


Figure 6: Schematic of immunohistochemical staining with ABC method.

#### 4.4.2 Procedure of Immunohistochemical staining

The immunohistochemical staining workflow started with deparaffinization and rehydration (table 3). Paraffin was dissolved and removed by the solvent xylene. Xylene was removed by the application of graded solutions of ethanol. Tissue samples were rehydrated in ethanol of graded concentrations and, finally, distilled water. To minimize staining intensity discrepancy, each immunohistochemical staining was performed with all slides needed at once.

One bullet point is that once immunohistochemical staining initiates, tissue samples during the process should remain wet all the time because if tissue samples were dried, nonspecific binding would occur and result in high background signal. To this end, for example, when tissue samples were incubated for a longer period, they should be kept in a wet chamber.



Table 3: Deparaffinization and rehydration

Step	Duration
xylene	10 min
xylene	10 min
xylene	10 min
xylene /Ethanol 50%/50%	5 min
Ethanol 100%	3 min
Ethanol 100%	3 min
Ethanol 96%	3 min
Ethanol 96%	3 min
Ethanol 70%	3 min
Ethanol 50%	3 min
Distilled water	3 min

After deparaffinization and rehydration, heat induced antigen retrieval (HIER) should be performed if necessary. Because during the processes of tissue fixation and paraffin-embedding, masking of antigen epitopes may occur, which could hinder primary antibodies from recognizing the antigen epitopes. Thus, the HIER procedure may be necessary to help uncover the masked antigens epitopes. But it is not necessary for all antigens. Consequently, an antibody optimization procedure should be established at first. In our lab, for HIER, tissue sections were placed in a plastic vessel and completely immersed in either citrate buffer (pH 6.0) or Tris(hydroxymethyl)aminomethane (Tris)/ ethylenediaminetetraacetic acid (EDTA) buffer (pH 9.0). The plastic vessel containing tissue sections was placed in a microwave oven till the buffer solution started to boil, and then the heating lasted for another 10 minutes without boiling. After that, the plastic vessel containing tissue sections was placed in a running tap water bath to get tissues slowly back to room temperature. Then tissue sections were washed in PBS 3 times, 5 minutes each time. Principally, tissue sections should be washed in PBS between 2 steps, but there is an exception, after serum blocking, tissue sections should be incubated with primary antibody directly without being washed in PBS.

In the next step, blocking was performed to reduce unspecific binding. In principle, the primary antibody binds specifically to the antigen. In practice, tissue samples may carry

endogenous Fc receptors that could recognize and bind to the primary antibody, resulting in unspecific binding. Therefore, blocking these endogenous Fc receptors using normal serum containing unspecific antibodies could reduce such unspecific binding. Usually, the animal from which the blocking serum is taken and the host in which secondary antibodies are raised should be of the same species.

Next, the slides were leaned to get rid of blocking serum, and the primary antibody incubation was performed. During this step, the primary antibodies were diluted in normal serum at optimal antibody concentration. Tissue sections were incubated with primary antibody at 4°C overnight. The primary antibodies used for immunohistochemical staining in this study were listed in table 4.

Table 4: Primary antibodies applied for immunohistochemical staining

antigen	species	dilution	HIER	supplier	purchase number	RRID	tissue samples
ALDH1L1	Rabbit	1:750	without	Abcam, UK	Ab87117	GR335 4022-1	Mouse
Laminin	Rabbit	1:300	Tris/EDTA	Abcam, UK	Ab11575	GR326 8366-1	Mouse
ALDH1L1	Rabbit	1:200	Citrate	Abcam, UK	Ab177463	GR33/9 6/2-1	Human
GFAP	Rabbit	1:250	Tris/EDTA	Abcam, UK	Ab68428	GR257 920-32	Human

The next day, peroxidase blocking was performed after primary antibody incubation. In this step, hydrogen peroxide (0.35%) was applied to incubate the tissue samples for 30 minutes. The reason for the application of peroxidase blocking is that tissues may contain endogenous peroxidase which could react with chromogen substrate and chromogen, leading to unspecific background staining. Hence, hydrogen peroxide should be applied to inactivate endogenous peroxidase [75,76] and ultimately minimize such unspecific staining.

After that, secondary antibody incubation was performed. After secondary antibodies were diluted in normal serum, tissue samples were incubated with the secondary

antibody solution for 1 hour at room temperature. The secondary antibodies used for immunohistochemical staining in this study were listed in table 5.

Table 5: Secondary antibodies applied for immunohistochemical staining

secondary antibody	dilution	supplier	purchase number	RRID
Goat anti-rabbit IgG	1:200	Vector Laboratories, USA	BA-1000	AB_2313606

The next step is the application of HRP coupled avidin-biotin complex. Tissue sections were incubated with HRP coupled avidin-biotin complex for 1 hour at room temperature. It is noteworthy that the ABC-HRP system should be prepared at least 30 minutes before its application.

Then the chromogen DAB was diluted with DAB substrate, and the tissue sections were stained with the DAB solution for 10 minutes. Afterwards, tissues were washed in tap water for several seconds followed by distilled water for 5 minutes. Hematoxylin staining was performed for 1 minute to visualize cell nuclei with blue color if it was appropriate, which was also referred to as nuclear counterstain. Afterwards, tissue sections went through the process of dehydration (Table 6) and were mounted by a mounting medium DePeX.

Table 6: Dehydration

Step	Duration
Distilled water	3 min
Ethanol 50%	3 min
Ethanol 70%	3 min
Ethanol 96%	3 min
Ethanol 96%	3 min
Ethanol 100%	3 min
Ethanol 100%	3 min
xylene /Ethanol 50%/50%	5 min
xylene	10 min
xylene	10 min

The protocol, including the whole procedure of immunohistochemical staining, was listed in table 7.

Table 7: Protocol of immunohistochemical staining

Step	Process
1	Deparaffinization and rehydration (Table 3).
2	HIER if necessary in Citrate or Tris/EDTA for 10 minutes (after HIER, all the slides should return to room temperature in running tap water bath).
3	Blocking with 5% normal serum for 1 hour.
4	Primary antibody incubation overnight at 4°C , but for omission of primary antibody control, the primary antibody solution was replaced by 5% normal serum.
5	Slides were washed in PBS 3 times, 5 minutes each time. The negative controls should be washed separately.
6	Peroxidase blocking with hydrogen peroxide (0.35%) for 30 minutes
7	Slides were washed in PBS 3 times, 5 minutes each time.
8	Secondary antibody incubation for 1 hour at 4°C.
9	Slides were washed in PBS 3 times, 5 minutes each time.
10	ABC-HRP incubation. ABC-HRP system should be prepared at least 30 minutes before its application.
11	Slides were washed in PBS 3 times, 5 minutes each time.
12	Staining with DAB for 10 minutes.
13	Slides were washed in tap water for a few seconds, then in distilled water for 5 minutes.
14	Nuclear counterstain with hematoxylin for 1 minute if appropriate (then slides were washed 1% HCL-Ethanol for 5 seconds, in tap water for 5 minutes, afterwards in distilled water for 3 minutes).
15	Dehydration (Table 6)
16	Mounting with a medium DePeX.
17	Drying in a fume hood

## 4.5 Immunofluorescence

### 4.5.1 Principle of immunofluorescent staining

Immunofluorescent staining is a technique that can be used to identify antigens or proteins in situ in tissue sections as well. Although there are some differences, it is similar to immunohistochemical staining because both techniques take advantage of specific immunoreactions. The principle of immunofluorescent staining is summarized

as follows:

- ◆ Primary antibody binds specifically to the targeting antigen in biological tissue.
- ◆ Fluorophore-conjugated secondary antibody binds specifically to the primary antibody.
- ◆ Under an epifluorescence microscope, fluorophores absorb short-wavelength high energy light (excitation) and emit long-wavelength low energy light (fluorescence). The emitted light can be captured and digitalized. In this way, antigens are eventually visualized.
- ◆ If needed, cell nuclei can be visualized by 4',6-diamidino-2-phenylindole (DAPI), a popular fluorescent dye that binds to DNA and presents with blue color.
- ◆ If 2 antigens need to be visualized simultaneously, 2 combinations of primary antibodies and secondary antibodies should be applied. Specifically, 2 kinds of primary antibodies raised in 2 animal species should be chosen. In contrast, 2 kinds of secondary antibodies taken from the same animal species can be applied. These 2 kinds of secondary antibodies are conjugated with differential fluorophores which give out light of different wavelengths or colors. In this case, the technique is referred to as double immunofluorescent staining.

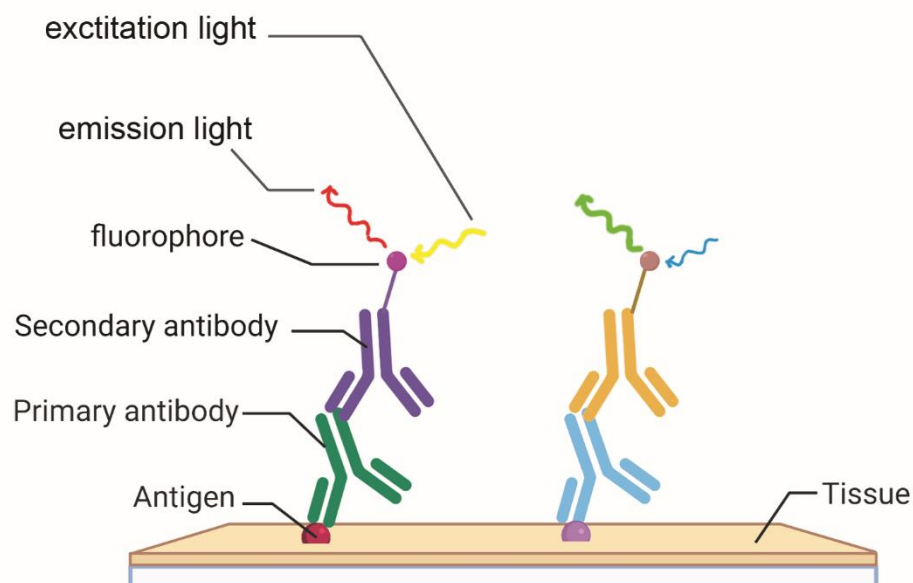


Figure 7: Schematic of double immunofluorescent staining.

#### 4.5.2 Procedure of double immunofluorescent staining

The double Immunofluorescent staining began with deparaffinization, and rehydration (table 2) followed by HIER if necessary and subsequently normal serum blocking, which was the same as steps during the immunohistochemical staining.

Then, incubation with 2 kinds of primary antibodies was performed at 4°C in a refrigerator overnight. When 2 kinds of primary antibodies were diluted into normal serum together, concentrations of both primary antibodies should be at their respective optimal dilution. The primary antibodies used for double immunofluorescent staining in this study were listed in table 8.

Table 8: Primary antibodies used for immunofluorescent staining

antigen	species	dilution	HIER	supplier	purchase number	RRID
ALDH1L1	Rabbit	1:1000	Tris/EDTA	Abcam, UK	Ab87117	GR33540 22-1
GFAP	Goat	1:500	Tris/EDTA	Sigma-Aldrich, USA	SAB25004 62-100UG	7478G2
CD31	Rat	1:20	Tris/EDTA	Dianova, Switzerland	DIA-310	201015/01

The next day, incubation with secondary antibodies was performed. The secondary antibodies were diluted with 5% normal serum at the optimal dilution. Secondary antibody incubation lasted for two hours at room temperature in a dark place to avoid bleaching. The secondary antibodies used for double immunofluorescent staining in this study were listed in table 9.

One bulletin point is that fluorescence signals may be damaged when fluorophores are exposed to light. Consequently, it is better to reduce light intensity and minimize exposure time to light when handling the secondary antibodies and in subsequent steps.

In this study, to help recognize the anatomical structure, nuclear counterstain was performed using DAPI. Finally, tissue sections were mounted. In this study, nuclear

counterstain and mounting were performed simultaneously because Fluoroshield containing mounting medium and DAPI was applied.

Table 9: Secondary antibodies used for immunofluorescent staining

secondary antibody	dilution	supplier	purchase number	RRID
Alexa Fluor 488-coupled donkey anti-rabbit IgG	1:250	Abcam, UK	ab150065	GR3225143-2
Alexa Fluor 594-coupled donkey anti-goat IgG	1:250	Abcam, UK	ab150132	GR3232359-4
Alexa Fluor 594-coupled donkey anti-rat IgG	1:250	Abcam, UK	ab150156	GR33585209-2

The protocol, including the whole procedure of double immunofluorescent staining, was listed in table 10.

Table 10: Protocol of double immunofluorescent staining

Step	Process
1	Deparaffinization and rehydration (Table 3).
2	HIER in Citrate or Tris/EDTA for 10 minutes if necessary (after HIER, all the slides should return to room temperature in running tap water bath).
3	Blocking with 5% normal serum for 1 hour.
4	Primary antibody incubation overnight at 4°C, but for omission of primary antibody control, the primary antibody was replaced by 5% normal serum. For each cross control, 1 kind of primary antibody was applied.
5	Slides were washed in PBS 3 times, 5 minutes each time. Each negative control should be washed separately.
6	Secondary antibody incubation for 1 hour at 4°C, but for each cross control, unmatched secondary antibody was applied.
7	Slides were washed in PBS 3 times, 5 minutes each time.
8	Nuclear counterstain and mounting with DAPI.
9	Drying and storage in a dark place.

## 4.6 Negative controls

Principally, immunohistochemical staining and immunofluorescent staining are based on specific immunoreactions. Several factors could cause unspecific bindings and false positive signals, including endogenous Fc receptors and endogenous hydrogen peroxidase as described previously. Different strategies can be utilized to verify whether the staining results are valid and accurate. Besides cellular staining type and distribution of positive signal, negative controls are helpful to verify staining specificity. Generally, positive signals are present in normally stained tissues and absent in negative controls, indicating that the results arise from specific bindings and are valid.

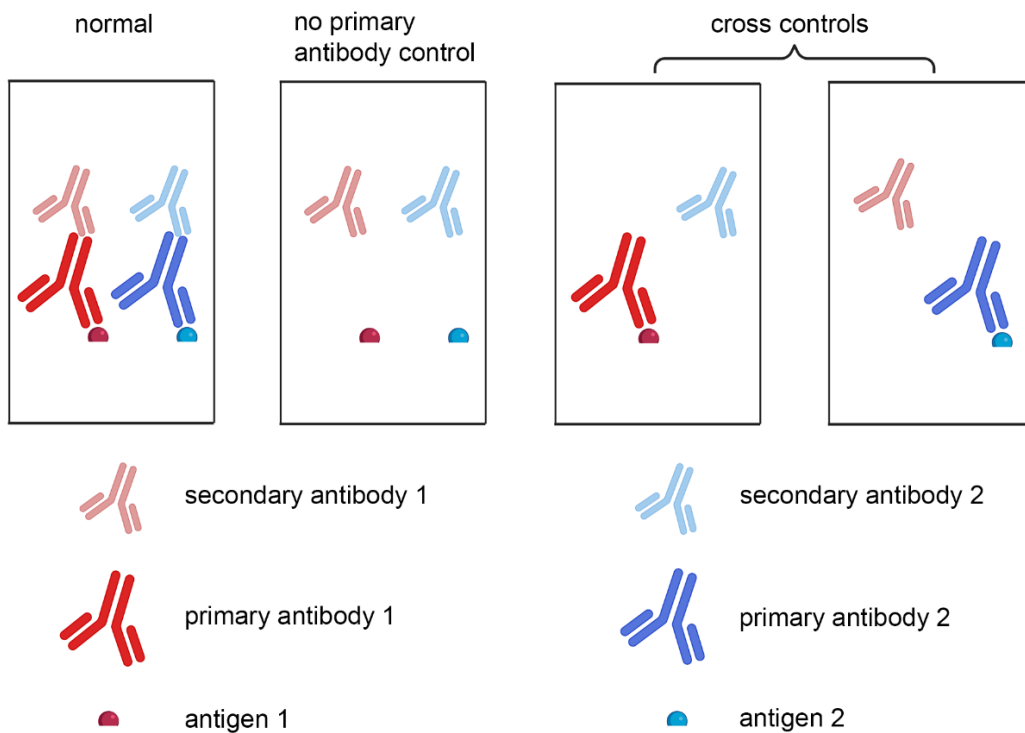


Figure 8: Schematic of negative controls in double immunofluorescent staining.

In omission of primary antibody control, the application of primary antibodies was omitted, while the secondary antibodies were applied. In each cross control, a combination of unmatched primary antibodies and secondary antibodies were applied.



In this study, omission of primary antibody was applied during immunohistochemical staining as negative controls. As its name implies, omission of primary antibody means the primary antibodies are not applied. If false positive signals could be observed in the negative controls, the false positive signals are usually considered to originate from unspecific bindings of secondary antibodies.

During the procedure of double immunofluorescent staining, omission of primary antibody and cross controls (figure 8) were applied as negative controls (figure 8). As shown in figure 8, cross controls were utilized to examine unspecific bindings of secondary antibody to unmatched primary antibody. To this end, combinations of unmatched primary antibodies and secondary antibodies were applied.

## **4.7 Digital Image Analysis**

All the sections stained in this study were digitalized using a Leica DM6 B microscope (Wetzlar, Germany) equipped with a Leica DMC6200 camera. Sections of each staining were digitalized under the microscope with the same settings to avoid discrepancy.

### **4.7.1 Quantification of single cellular area**

Principally, different kinds of cells usually have different cellular sizes and areas. Astrocytes are larger than other glial cells and neurons. To investigate whether these cells with weak intensity of anti-ALDH1L1 immunohistochemical staining were astrocytes or not, their cellular areas were measured, and then these data were compared with data of astrocytic cellular areas in publications. If these cellular areas with weak ALDH1L1 staining intensity were in line with data of astrocytic areas in publications, these cells with low ALDH1L1 expression would be proven to be astrocytes indeed.

To this end, 50 weakly stained cells by anti-ALDH1L1 staining from 3 rodent brain tissues were identified and included. Cellular areas of these 50 cells were measured.

At the same time, I found that there were no reliable data regarding cellular area of astrocytes in publications. But some literatures offered images of astrocytes allowing for measuring cellular areas. In the end, 7 images of astrocytes from 3 publications were included and the area of these cells were quantified [77–79].

Briefly, cellular areas of 2 groups were measured in this study. One group of 50 astrocytes with weak anti-ALDH1L1 staining intensity and the other group of 7 astrocytes from 3 publications were included. The open-source software Fiji/ImageJ (1.53i, NIH, Bethesda, MD, USA) was applied to measure the cellular areas of astrocytes. Detailed steps were as follows.

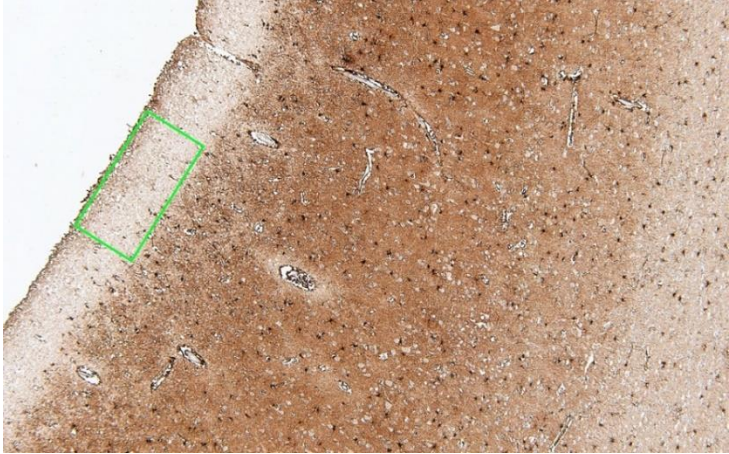
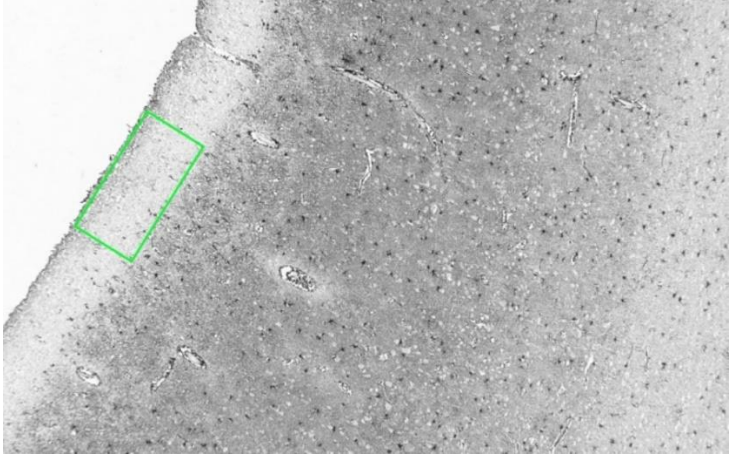
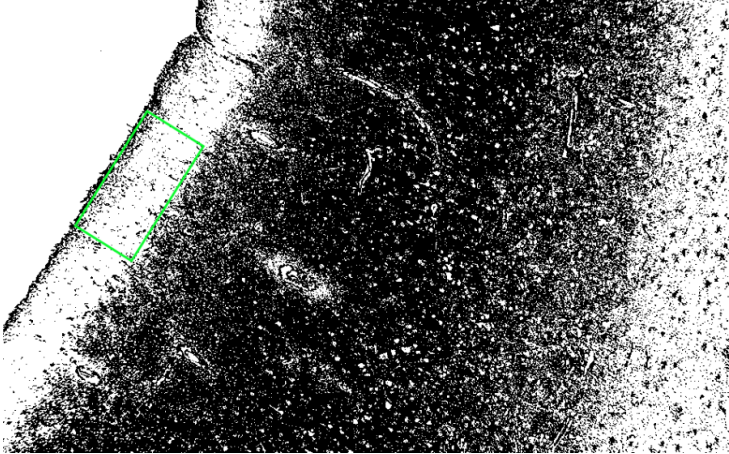
- ◆ Set measurements and check “area”
- ◆ Set scale and convert the calibration from pixel to micron.
- ◆ Use “Polygon Selections” to demarcate the border of each targeting cell.
- ◆ “Measure” and get the data.

#### **4.7.2 Quantification of staining intensity**

The immunohistochemical staining intensity were evaluated using the open-source software ImageJ (1.53i, NIH, Bethesda, MD, USA) with densitometrical algorithm. The staining intensities of several regions of interest (ROIs) were quantified, including the superficial region of cortex, deep region of cortex, perivascular regions, and medium corpus callosum. Detailed steps were as follows.

- ◆ Set measurements, check “area fraction”.
- ◆ Select the ROI.
- ◆ Convert the colorized image to an 8-bit grey image.
- ◆ Convert the image to black&white image.
- ◆ Measure the density of black pixels in the ROI and get the data offered as percentage of area.

Table 11: Quantification of staining intensity

Steps	Diagram	Annotation
<p>“Polygon Selections”</p>		<p>Select superficial region of cortex as ROI.</p>
<p>“Image type” “8-bit”</p>		<p>Convert the colorized image to an 8-bit grey image.</p>
<p>“Image” “ Adjust” “Threshold”</p>		<p>Convert the image to black&amp;white image, then measure the density of black pixels (% area) in the ROI.</p>

### 4.7.3 ROIs

In this study, when quantifying the staining intensities and counting cell numbers, several ROIs were included and applied. In human brain sections, superficial regions of cortex, deep regions of cortex (figure 9, A) were included as ROIs when evaluating the cortical staining intensity.

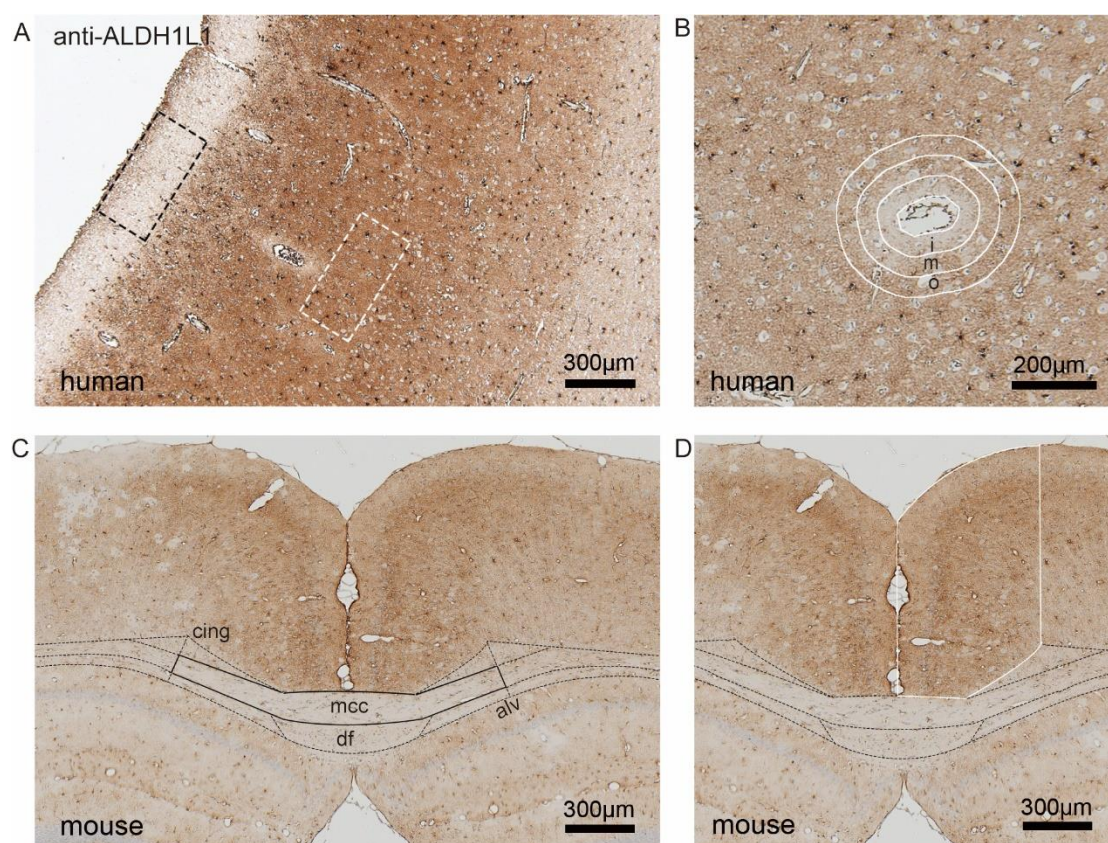


Figure 9: Schematic of ROIs.

(A) In the human cortex, superficial region of cortex (dashed black line) and deep region of cortex (dashed white line) were selected as ROIs. (B) Concentric perivascular regions (solid white line) were utilized as ROIs. (C) Medium corpus callosum (solid black line) was identified as ROIs. (D) Cortex (solid white line) were marked as ROIs. Abbreviations = i: inner concentric region, m: medium concentric region, o: outer concentric region, cing: cingulum, mcc: medium corpus callosum, df: dorsal fornix, alv: alveus.

When analyzing the staining intensities in the concentric perivascular regions (figure 9, B), after the border of the blood vessel was outlined, a macro was applied to label concentric perivascular circles. In this way, 3 concentric perivascular regions were

established, including inner, medium, and outer concentric perivascular regions.

The rodent brain sections at the level of 285 according to the mouse brain atlas published by Sidman et al. were applied. Medium corpus callosum (figure 9, C) was selected as ROIs when quantifying the staining intensity of ALDH1L1. Part of the cortex (figure 9, D, enclosed by 5 lines, including middle line, borders of pia matter, boundaries of medium corpus callosum and cingulum, a line through the tip of cingulum and parallel to middle line) was defined as ROIs when quantifying the cell density of astrocytes.

#### **4.7.4 Quantification of cell density**

Cell density in the ROIs was quantified using the open-source software ImageJ (1.53i, NIH, Bethesda, MD, USA). The ROIs were manually outlined. Areas of the ROIs were measured. Astrocytes within the ROIs were marked and counted by an experimenter blinded to the groups. In the end, cell densities were calculated and given as cells/mm<sup>2</sup>.

### **4.8 Statistical Analysis**

The statistical analyses were performed using GraphPad Prism 8 (GraphPad Software Inc., San Diego, CA, USA). The data were given as arithmetic means  $\pm$  standard error of the mean (SEM). First, normality test was performed to evaluate whether the data were in accordance with Gaussian distribution, then t-test, Mann-Whitney test, or one-way ANOVA was applied, if appropriate. The specific statistical procedures applied for the analyses were provided in the respective figure legends. The following symbols were used to indicate the level of significance: \*  $p \leq 0.05$ , \*\*  $p \leq 0.01$ , \*\*\*  $p \leq 0.001$  and ns (=not significant)  $p > 0.05$ .

## 5. Results

### 5.1 Protoplasmic and fibrous pattern

At first, it should be evaluated that whether the applied antibody could visualize astrocytes in human and murine brain tissues. To this end, 1 human brain section and 1 murine brain section were processed for anti-ALDH1L1 immunohistochemistry and evaluated for the presence of astrocytes.

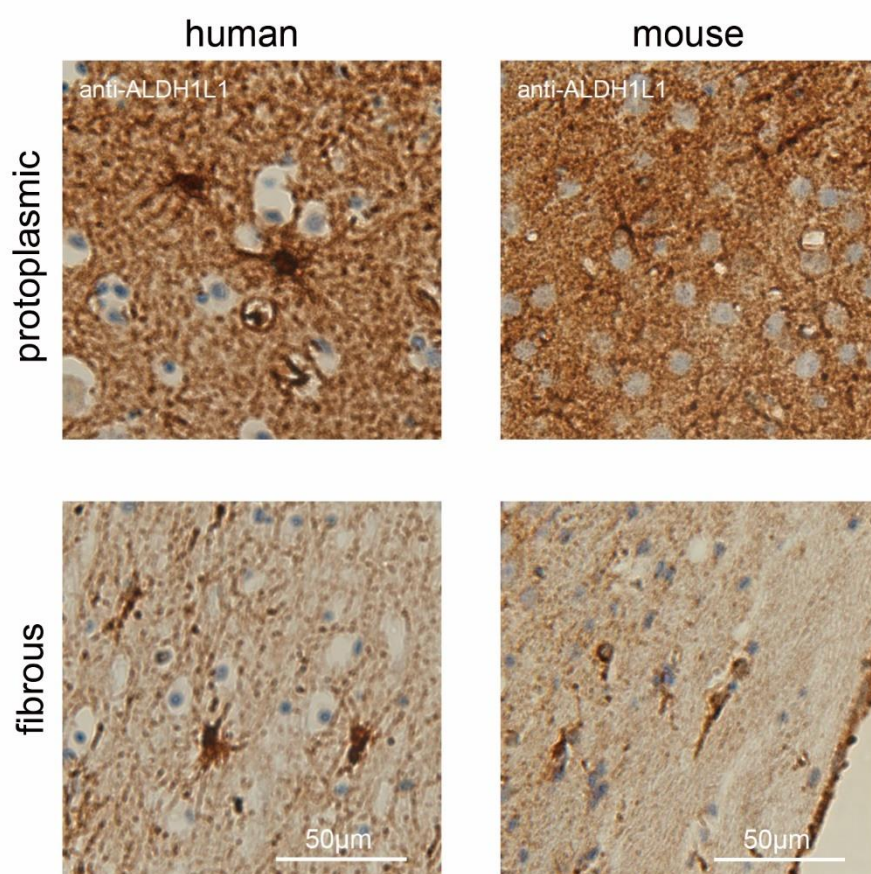


Figure 10: Astrocytes visualized by immunohistochemical staining for ALDH1L1.

Protoplasmic and fibrous astrocytes located in the grey matter and white matter respectively were visualized by immunohistochemical staining for ALDH1L1. Human astrocytes possessed more processes and larger volumes than murine astrocytes.

As shown in figure 10, protoplasmic and fibrous astrocytes in the grey matter and white matter respectively were well visualized by the anti-ALDH1L1 antibody. Protoplasmic astrocytes exhibited a starlike shape with branched bushy processes, whereas fibrous type exhibited relatively fewer processes. Human astrocytes were larger than murine astrocytes in terms of cellular size and exhibited more complex morphology.

## **5.2 ALDH1L1 expression in human cortex**

To investigate the expression of ALDH1L1 by astrocytes in the human cortex, 3 brain sections from 3 control human body donors were processed for anti-ALDH1L1 immunohistochemical staining. As shown in Figure 11, in the cortex of human brain, the diffuse high staining intensity may be attributed to large amounts of astrocytic processes. Whereas, in the superficial cortical regions near the glia limitans superficialis, decreased intensity of anti-ALDH1L1 staining was observed, and the regions around some blood vessels displayed weak staining intensity as well. In this case, the expression of ALDH1L1 by astrocytes differed in a region-dependent manner to some extent.

To evaluate whether these staining intensity differences were significant or not, staining intensity in superficial regions and deep layers of cortex as well as the concentric perivascular regions was quantified and statistically analyzed. As shown in Figure 12, the results indicated a significant difference in anti-ALDH1L1 staining intensity between superficial regions and deep regions of the cortex, and staining intensity differed significantly between concentric perivascular regions.

However, not all perivascular regions showed weak staining intensity, at least regions around some blood vessels displayed relatively normal staining intensity (data not shown).

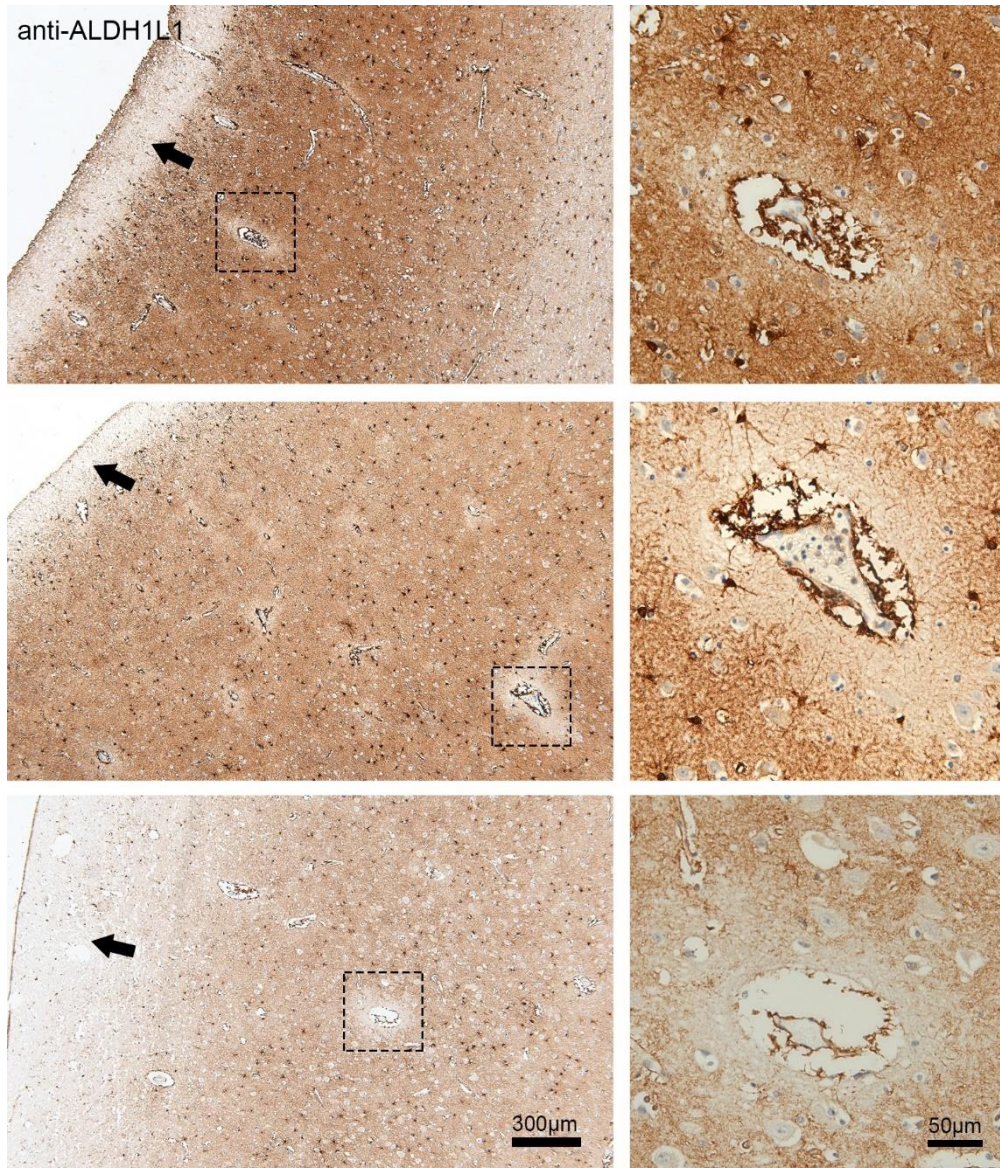


Figure 11: ALDH1L1 expression in human brain cortex.

Images of immunohistochemical staining for ALDH1L1 with brain tissues from 3 control humans. Superficial cortical regions (arrows) and some perivascular regions (dashed line) presented low staining intensity. On the right were magnified images of perivascular regions.



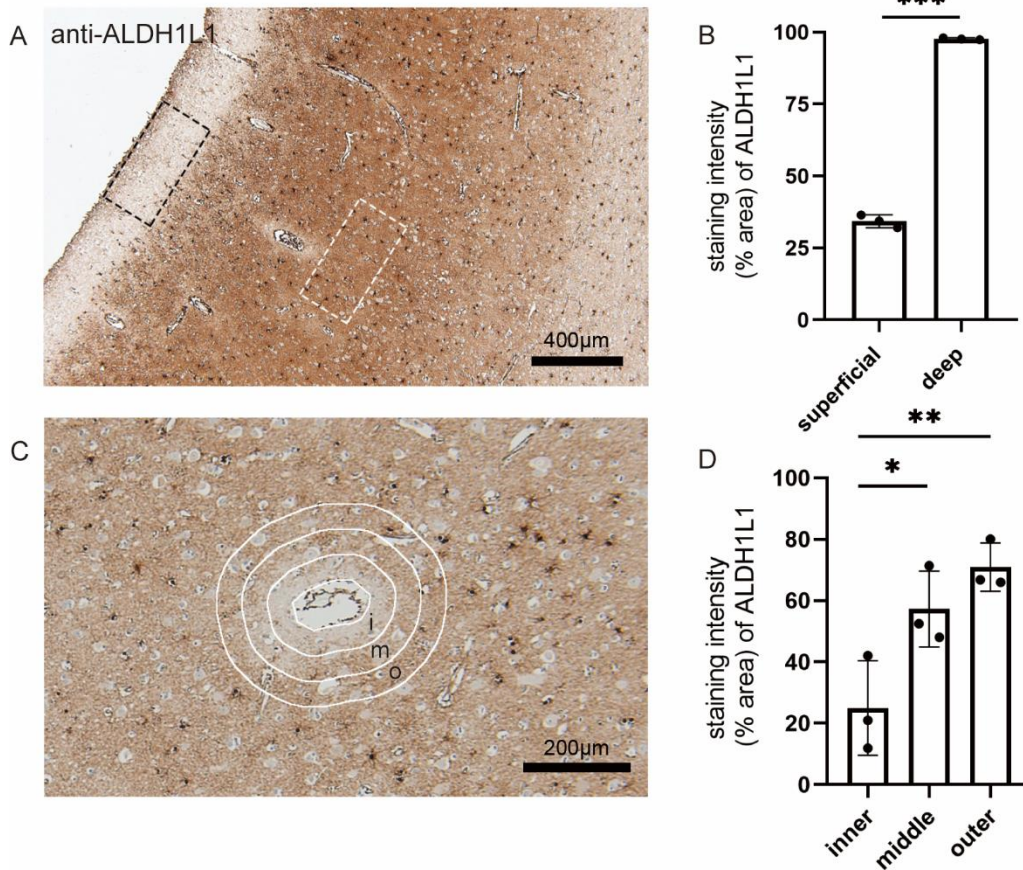


Figure 12: Anti-ALDH1L1 staining intensity in the human brain cortex.

(A) Anti-ALDH1L1 staining intensity in superficial regions (dashed black line) and deep layers of cortex (dashed white line) was quantified, and the statistical analysis (B) indicated a significant difference,  $n = 3$ ,  $*** p < 0.001$ , paired t-test. (C) Anti-ALDH1L1 staining intensity in perivascular regions was quantified, the statistical analysis (D) indicated a significant difference in staining intensity between perivascular regions,  $i =$  inner perivascular region,  $m =$  medium perivascular region,  $o =$  outer medium perivascular region perivascular region,  $n=3$ ,  $* p < 0.05$ ,  $** p < 0.01$ , one-way ANOVA test.

### 5.3 GFAP expression in human cortex

To investigate the astrocytic expression of GFAP in human cortex, 3 brain sections from 3 control humans were processed for anti-GFAP immunohistochemical staining. As shown in Figure 13, under physiological conditions, not all astrocytes were visualized by immunohistochemical staining for GFAP. In general, astrocytes in superficial regions of the cortex (near the glia limitans superficialis) and perivascular regions (near the glia limitans perivascularis) were GFAP positive, while most of the

other cortical astrocytes were GFAP negative.

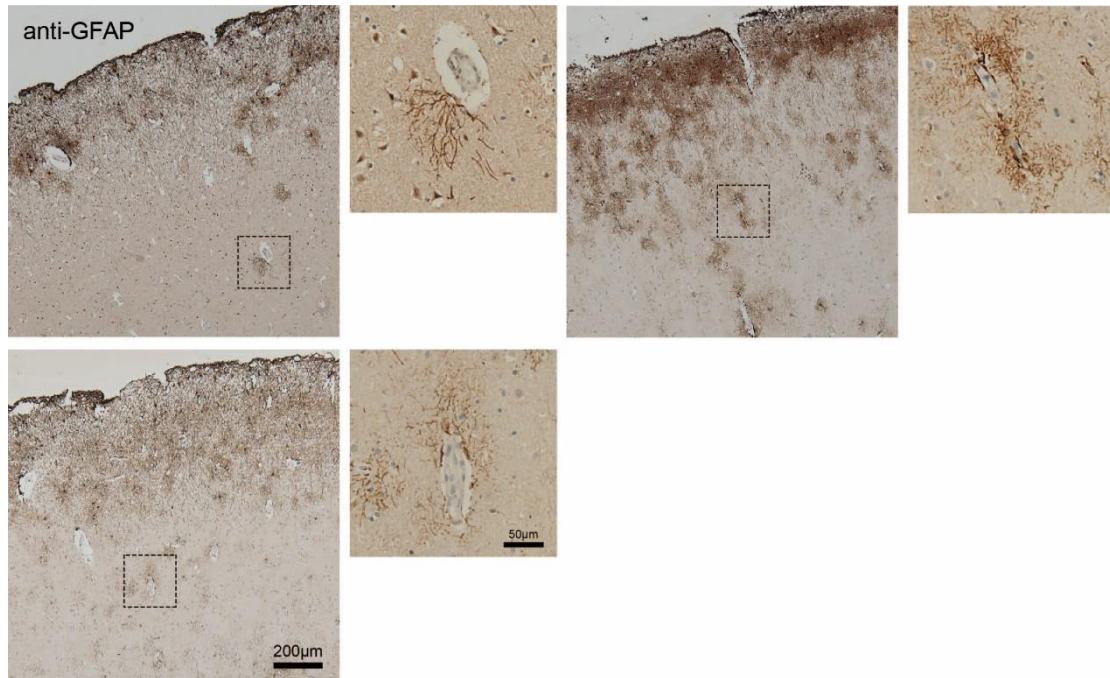


Figure 13: GFAP expression in human brain cortex.

Images of immunohistochemical staining for GFAP with brain tissues from 3 control humans. Astrocytes in superficial layers of cortex and around some blood vessels (dashed line, magnified images on the right) could be visualized by immunohistochemical staining for GFAP.

## 5.4 ALDH1L1 expression in murine cortex

To investigate the expression of ALDH1L1 by astrocytes in the murine cortex, 6 brain sections from 3 control mice were processed for anti-ALDH1L1 immunohistochemical staining. As shown in Figure 14, in the mouse brain cortex, astrocytes exhibited protoplasmic morphology, and their somas and stem processes were well visualized by the anti-ALDH1L1 antibody.

Besides these astrocytes with protoplasmic morphology, weakly stained areas (Figure 5, Figure 14) were found in the murine cortex. In the center of each weakly stained area, the soma and stem processes were positively marked, implying that some astrocytes do not express ALDH1L1 at the periphery but just within the central compartments.

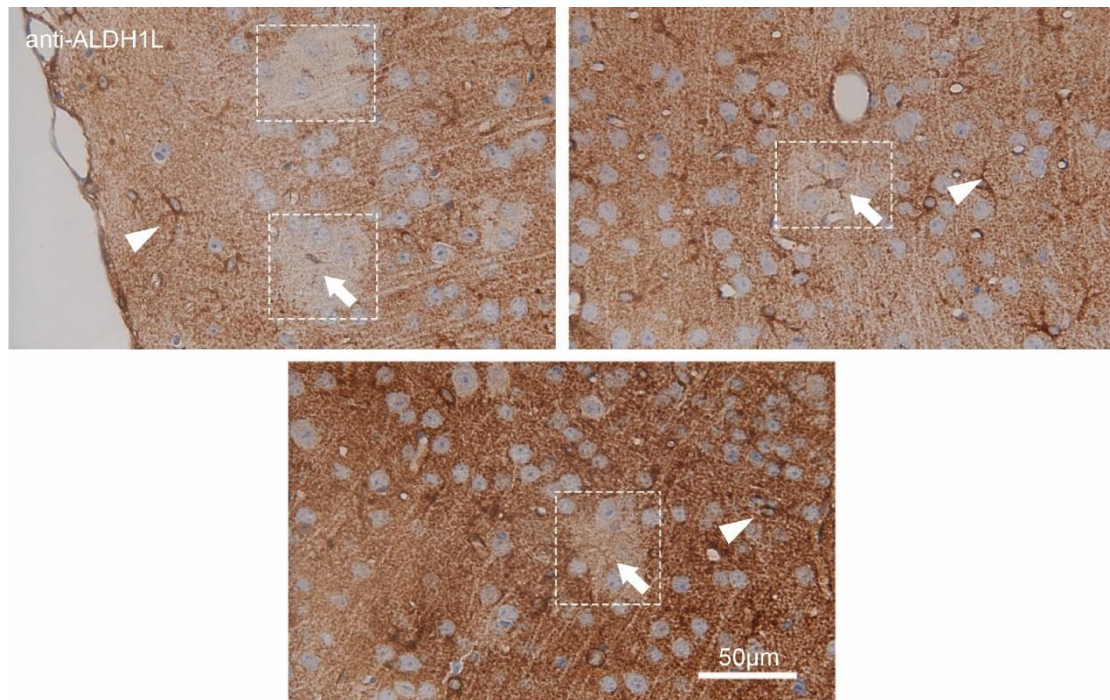


Figure 14: Astrocytes in mouse brain cortex.

Images of immunohistochemical staining for ALDH1L1 with brain tissues from 3 control mice. Astrocytes in the cortex of the mouse brain exhibited protoplasmic morphology (arrowheads). Weakly stained areas (dashed white line) with low staining intensity were present in the cortex. In the center of each weakly stained area, the soma and stem processes were positively stained (arrows).

## 5.5 Cellular areas of astrocytes

In principle, different kinds of cells possessed different cellular sizes. Astrocytes possessed larger cellular sizes than other glial cells and neurons. Consequently, to investigate whether the above-mentioned weakly stained cells were indeed astrocytes, I measured the cellular areas of these weakly stained cells. Then the data were compared with the data of astrocytic cellular areas in publications (see material and methods section for more detailed information).

For this purpose, 6 stained brain sections from 3 control mice were digitalized. 50 weakly stained cells by anti-ALDH1L1 staining were identified and included, overlapped cells with weak staining intensity were excluded. The cellular areas were measured using open source software, ImageJ (1.53i, NIH, Bethesda, MD, USA). Data of 50 cellular areas were listed in table 12 (left column).

I did not find reliable data regarding the area of astrocytes in literatures. However, in some publications, the authors provided images of protoplasmic astrocytes with a scalebar. Therefore, I measured cellular areas of these astrocytes by using the provided scalebars on my own. The data of astrocytic areas were listed in table 12 (right column).

Table 12: Cellular areas of astrocytes

cellular area of weak ALDH1L1 expression ( $\mu\text{m}^2$ )	measured area of astrocyte from literature ( $\mu\text{m}^2$ )
1434.036	1485.875
1203.055	1642.750
1211.917	1075.250
1386.921	1499.082
1327.020	1468.538
1186.322	1064.294
1942.164	1487.143
1057.226	
1336.162	
1522.163	
1304.875	
1252.369	
1132.415	
1297.694	
1432.440	
1906.801	
1822.189	
1705.943	
1441.756	
1280.487	
1242.882	
1192.575	
834.740	
953.422	
1448.720	
1167.757	
1569.170	
1089.052	
1314.125	
1090.391	
819.603	
1336.507	
1455.038	
1130.410	
1200.554	
1411.158	

cellular area of weak ALDH1L1 expression ( $\mu\text{m}^2$ )	measured area of astrocyte from literature ( $\mu\text{m}^2$ )
1217.028	
1379.806	
1625.622	
1281.263	
1232.725	
1074.001	
1586.464	
1401.131	
770.505	
1141.817	
1918.445	
981.648	
1461.938	
1595.089	

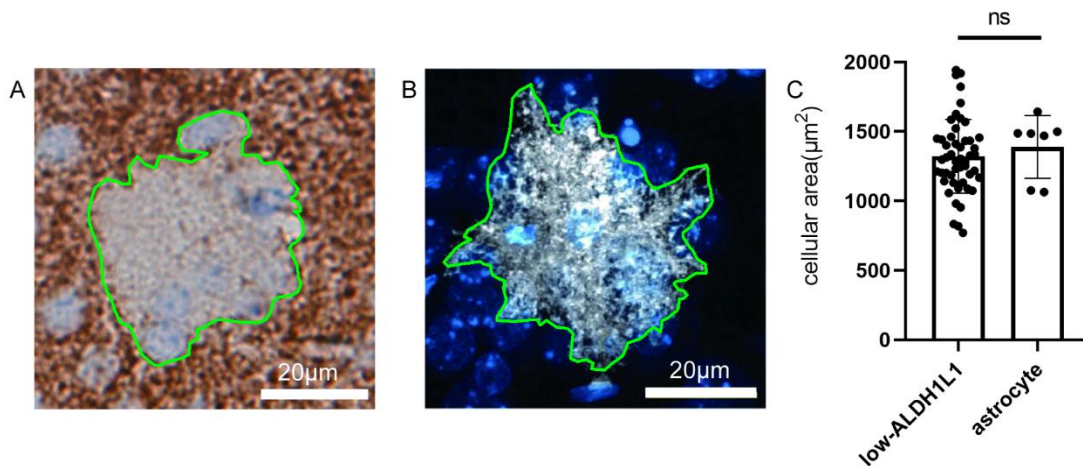


Figure 15: Cellular areas of murine astrocytes.

(A) Image of a weakly stained cell. The cellular borders were demarcated to measure the cellular area. (B) Image of a protoplasmic astrocyte modified from literature [78]. (C) Analyses of cellular areas. Results indicated that there was no significant difference between the data of the 2 groups. ns = not significant, Mann-Whitney test.

As shown in Figure 15, the cellular borders were outlined, and cellular areas were measured. Statistical analyses were performed to test whether the data of the 2 groups were consistent with each other. Results indicated that the mean cellular area of the 2 groups were  $1322 \pm 37.56 \mu\text{m}^2$  and  $1389 \pm 85.32 \mu\text{m}^2$ , and no significant difference was found between the data of 2 groups. These weakly stained cells possessed

cellular areas comparable to astrocytic cellular areas, implying these weakly stained cells were indeed astrocytes.

The other way to prove these cells with weak staining intensity of ALDH1L1 were indeed astrocytes was using double immunofluorescent staining for 2 astrocytic markers, namely ALDH1L1 and GFAP. In this way, astrocytes were visualized by 2 different fluorescent signals corresponding to ALDH1L1 and GFAP respectively. If the cells which presented weak ALDH1L1 signal showed a clear GFAP signal, we can assume these cells were indeed astrocytes.

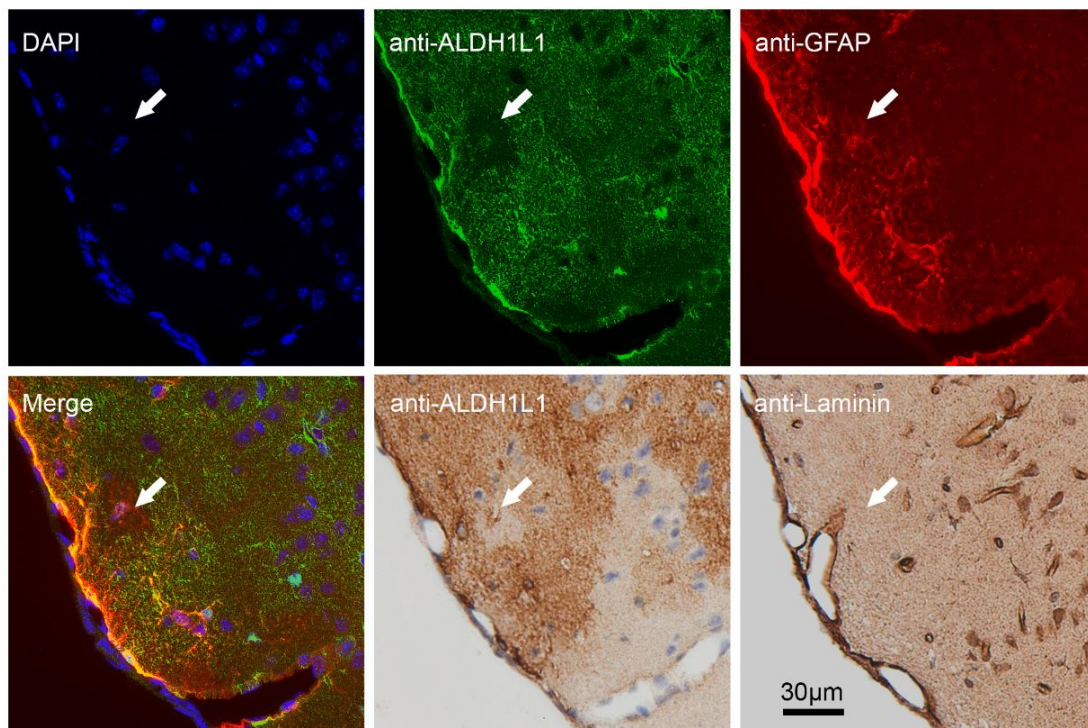


Figure 16: Image of consecutive sections stained for ALDH1L1, GFAP, and Laminin.

The double immunofluorescent staining labeled an astrocyte whose soma and stem processes were obviously visualized by the anti-GFAP antibody, while only the soma was weakly labeled by the anti-ALDH1L1 antibody. Immunohistochemical staining for ALDH1L1 revealed reduced staining intensity of the same astrocyte as well. A blood vessel visualized by immunohistochemical staining for laminin seemingly went through the territory of the astrocyte.

Given that some perivascular regions displayed significantly weak staining intensity of ALDH1L1 in human cortex, I tried to investigate whether the low ALDH1L1 expression was related to blood vessels in the murine cortex as well. I did the anti-Laminin

immunohistochemical staining to visualize blood vessels.

In order to localize and label the very same astrocyte, 3 consecutive sections were processed for double immunofluorescent staining (ALDH1L1 and GFAP), anti-ALDH1L1 immunohistochemical staining, anti-Laminin immunohistochemical staining, respectively.

As shown in Figure 16, one cell was labeled by double immunofluorescent staining for ALDH1L1 and GFAP. Only the soma was weakly marked by the fluorescent signal of ALDH1L1, which was consistent with the result of weak immunohistochemical staining intensity of ALDH1L1, indicating low expression of ALDH1L1 by the cell at its periphery. However, the soma and stem processes were clearly visualized by the immunofluorescent signal of GFAP, indicating the cell with low ALDH1L1 expression was indeed an astrocyte. Moreover, a blood vessel visualized by anti-Laminin immunohistochemical staining went through the territory of the astrocyte with weak ALDH1L1 expression, implying a close relationship between the blood vessel and this particular astrocyte.

Finally, in two different ways, including cellular areas comparison, and double immunofluorescent staining for ALDH1L1 and GFAP, these cells in murine cortex with low ALDH1L1 expression were confirmed to be astrocytes.

## **5.6 Relations between astrocytes with low ALDH1L1 expression and blood vessels**

As shown in Figure 16, a blood vessel went through the territory of the particular astrocyte with low ALDH1L1 expression, implying a close relation between them. To further investigate whether astrocytic low ALDH1L1 expression was associated with blood vessels, I did a double immunofluorescent staining which visualized astrocytes with the low ALDH1L1 expression and blood vessels simultaneously.

6 brain sections from 3 mice were used to perform double immunofluorescent staining for ALDH1L1 and CD31. CD31, a marker of endothelial cells, was used to mark blood

vessels. As shown in the upper 3 images (Figure 17), regional loss of ALDH1L1 signal around blood vessels could be clearly identified, indicating close relations between regional expression loss of ALDH1L1 by astrocytes and blood vessels. In the lower 3 images (Figure 17), astrocytes displayed regular ALDH1L1 expression around blood vessels, implying not all astrocytes around blood vessels were with low expression of ALDH1L1.

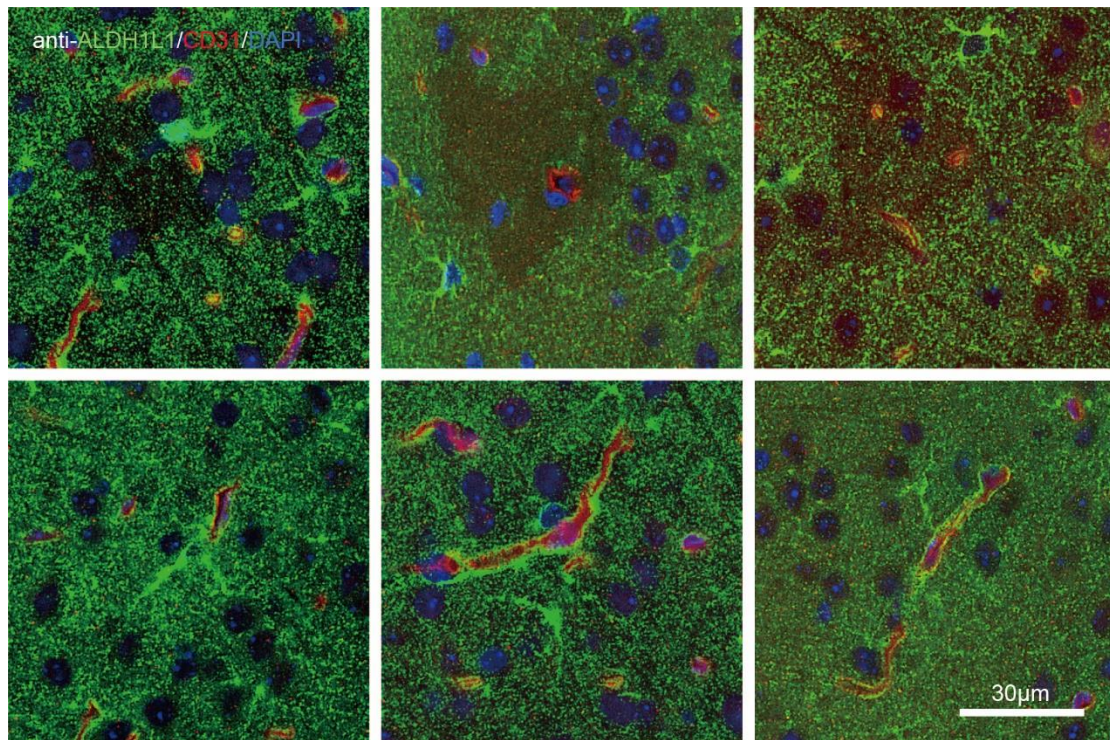


Figure 17: Image of double immunofluorescent staining for ALDH1L1 and CD31.

Double immunofluorescent staining for ALDH1L1 and CD31 was performed to label astrocytes and blood vessels simultaneously with brain tissues from 3 mice. The upper 3 images revealed regional loss of ALDH1L1 signal around blood vessels, while the lower 3 images demonstrated astrocytes with regular ALDH1L1 expression around blood vessels.

## 5.7 ALDH1L1 expression in post-mortem MS tissues

To investigate the ALDH1L1 expression under the condition of MS, 3 post-mortem brain sections from 3 MS patients were immunohistochemically stained for ALDH1L1. 3 brain sections from 3 control human were stained for ALDH1L1 as well to check whether expression changes of ALDH1L1 existed compared with MS.



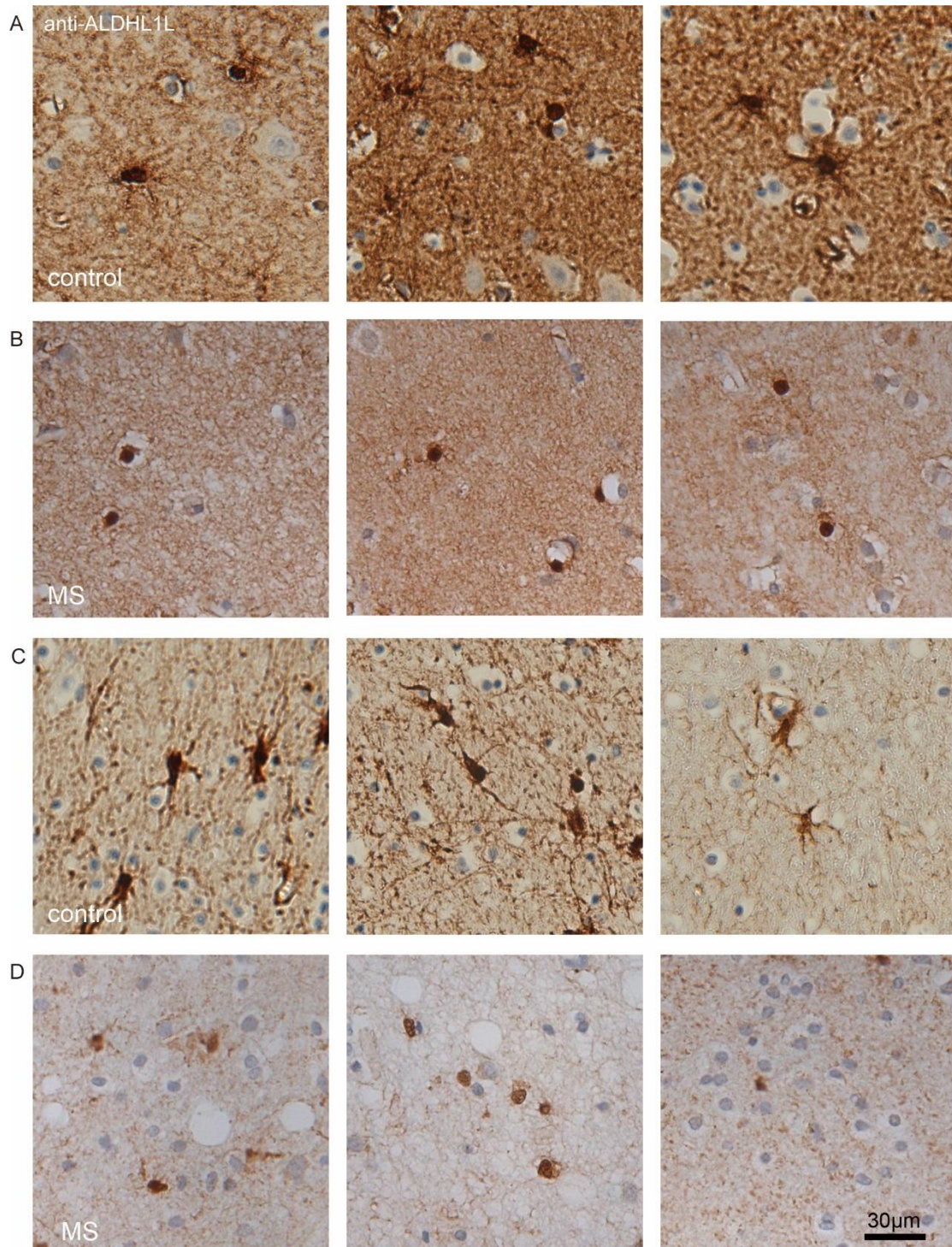


Figure 18: Image of astrocytes in control human and MS brain tissues.

Astrocytes visualized by immunohistochemical staining for ALDH1L1 with tissues from 3 control humans and 3 MS patients. (A) Image of astrocytes in the cortex of control tissues. (B) Image of astrocytes in the cortex of MS tissues. (C) Image of astrocytes in the white matter of control tissues. (D) Image of astrocytes in the white matter of MS tissues.

As shown in Figure 18, in the cortex and white matter of control tissue, the somas and stem processes of astrocytes were visualized by immunohistochemical staining for ALDH1L1. The morphology of protoplasmic and fibrous astrocytes was identified. In the cortex and white matter of MS tissue, the somas of some astrocytes were still visualized by the anti-ALDH1L1 antibody, but the morphology of stem processes was hard to identify. Under the condition of MS, cellular expression of ALDH1L1 seemed concentrated in the somas of some astrocytes.

## 5.8 Astrocytic ALDH1L1 expression in cuprizone models

To investigate the ALDH1L1 expression under the condition of cuprizone models, 20 brain sections from 20 mice of control, 1-week cuprizone, 3-week cuprizone and 5-week cuprizone groups were immunohistochemically stained for ALDH1L1.

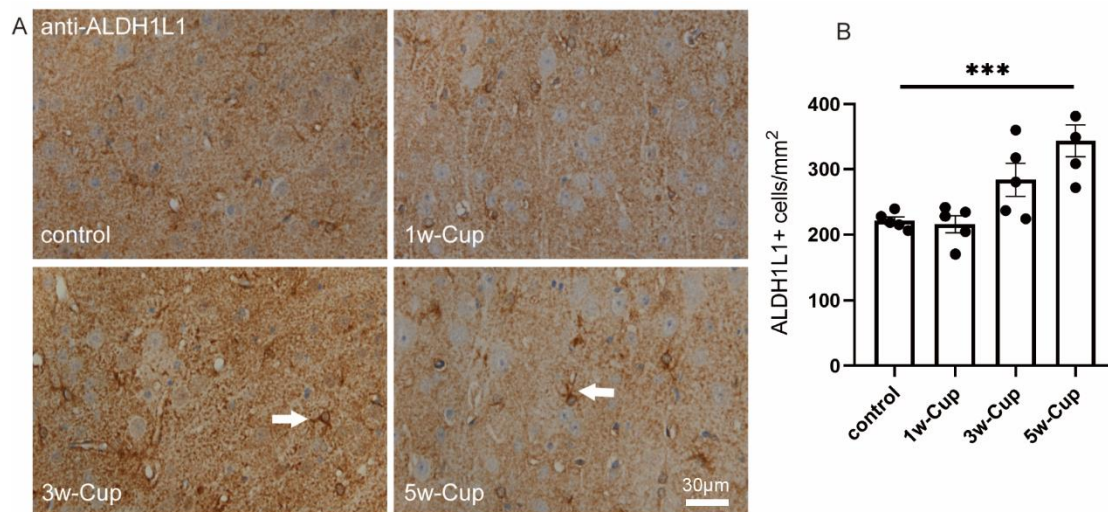


Figure 19: Image of astrocytes in the cortex of cuprizone models.

(A) Schematic of ALDH1L1 expression in the cortex of different groups. In the 3w-Cup and 5w-Cup groups, some astrocytes presented thicker processes (arrows) compared with control group. (B) Analysis of ALDH1L1+ cell density in 4 groups. The results indicated that the ALDH1L1+ cell densities differed significantly between control group and 5-week cuprizone intoxication group, w-Cup: week-cuprizone, one way ANOVA test.

As shown in Figure 19, in 3-week and 5-week cuprizone groups, some cortical astrocytes exhibited thicker processes compared with control group based on anti-ALDH1L1 immunohistochemical staining. ALDH1L1+ cell densities in the cortex (ROI shown in Figure 9, D) of different groups were analyzed. The results revealed that compared with the control group, ALDH1L1+ cell densities differed significantly in the 5-week cuprizone group, but not in the 1-week and 3-week cuprizone group.

As shown in Figure 20, staining intensity changes were identified in the medium corpus callosum of different groups. The statistical analysis results revealed that compared with the control group, anti-ALDH1L1 staining intensities differed significantly in the 5-week cuprizone intoxication group, but not in the 1-week and 3-week cuprizone intoxication groups. Anti-ALDH1L1 staining intensity changes indicated different levels of astrogliosis in these groups.

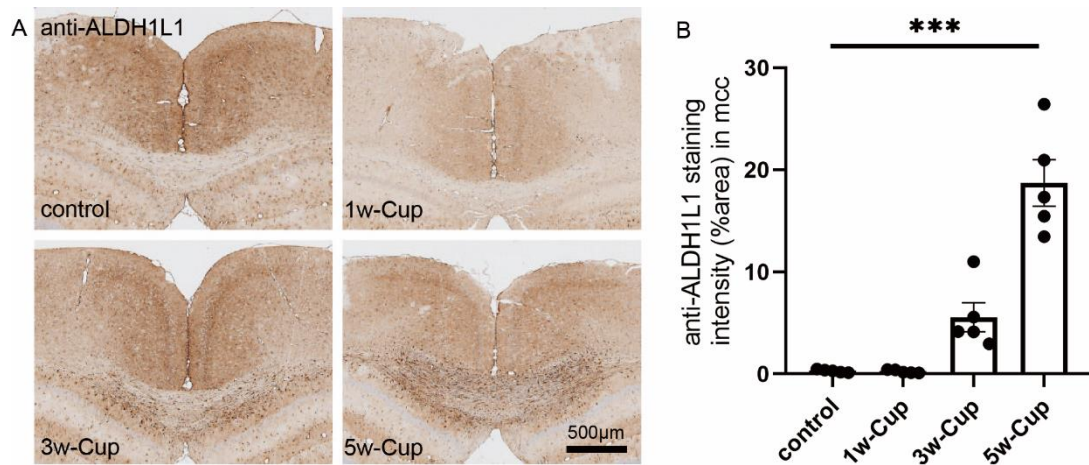


Figure 20: Astroglial staining in the medium corpus callosum of cuprizone models.

(A) Schematic of anti-ALDH1L1 staining intensity in 4 groups. (B) Analysis of anti-ALDH1L1 staining intensities in 4 groups indicated the expression level of ALDH1L1 in medium corpus callosum differed significantly between control group and 5-week cuprizone intoxication group, w-Cup: week-cuprizone, one way ANOVA test.

## 5.9 Negative controls

To verify the validity of the staining, I performed in parallel negative controls when

performing the staining in this study. Specifically, omission of primary antibody controls were adopted when immunohistochemical staining was performed. Omission of primary antibody and cross controls were adopted when double immunofluorescent staining was performed.

As shown in Figure 21 (A), astrocytes were visualized by anti-ALDH1L1 immunohistochemical staining, and the nuclei were counterstained. When primary antibodies were omitted, only the nuclei were counterstained.

As shown in Figure 21 (B), astrocytes were labeled by two markers, ALDH1L1 and GFAP, through double immunofluorescent staining, and the nuclei were marked by DAPI. In primary antibody omission control where the application of primary antibodies was omitted, and in cross controls where unmatched primary antibodies and secondary antibodies were applied, only the nuclei were marked by DAPI, both ALDH1L1 and GFAP signals were absent.

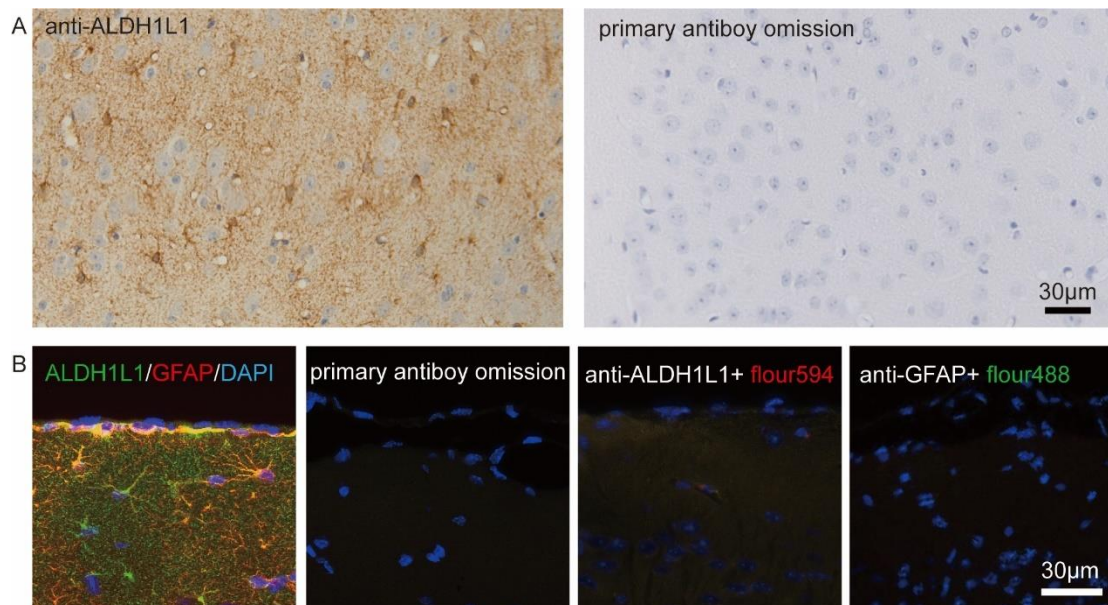


Figure 21: Schematic of negative controls.

(A) Images of immunohistochemical staining for ALDH1L1 and primary antibody omission control respectively. (B) Images of double immunofluorescent staining for ALDH1L1 and GFAP, primary antibody omission control, and cross controls respectively. All these 4 Images were merged images captured under the same settings. In primary antibody omission control, the application of primary antibodies was omitted. In cross controls, unmatched combinations of primary antibodies and secondary antibodies (rabbit anti-mouse ALDH1L1 + Alexa Fluor 594-coupled donkey anti-goat IgG, goat anti-rat GFAP + Alexa Fluor 488-coupled donkey anti-rabbit IgG) were applied.

## 6. Discussion

### 6.1 The expression of ALDH1L1 by astrocytes

Both protoplasmic and fibrous astrocytes could be well visualized by anti-ALDH1L1 antibody. As shown in this study, the astrocytic expression of ALDH1L1 exhibited some properties in a region-dependent manner, at the same time, the expression of ALDH1L1 and GFAP by astrocytes seemed quite different.

In humans, astrocytes in superficial regions of the cortex and in some perivascular regions exhibited decreased expression of ALDH1L1. In mice, astrocytes in superficial regions of the cortex did not show regional expression loss of ALDH1L1, whereas reduced expression of ALDH1L1 around some blood vessels did exist.

In human brain tissues, astrocytes in cortical regions near the glia limitans superficialis and near the glia limitans perivascularis expressed GFAP, and most of the other cortical astrocytes were GFAP negative. In rodent brain tissues, it has been demonstrated that the expression of GFAP was similar to that in human brain tissues [80].

To some extent, the expression of ALDH1L1 and GFAP exhibited contrary characteristics in a region-dependent manner, although the contrary tendency was not strictly rigid at regional and cellular levels.

It has been shown that in GFAP  $-/-$  mice, the function and morphology of BBB were affected severely. Consequently, the expression of GFAP has been associated with the integrity of BBB [81]. Therefore, regional expression of GFAP by astrocytes near the glia limitans superficialis and the glia limitans perivascularis may be a result of the involvement of astrocytes and GFAP in the maintenance of BBB.

In the cortex and white matter of MS brain tissues, the expression of ALDH1L1 by some astrocytes seemed concentrated in the somas, while the processes, including stem processes, displayed much lower ALDH1L1 expression.

In cuprizone models, reactive astrocytes exhibited morphological changes, including

enlarged somas and stem processes [69]. These morphological changes made these reactive astrocytes seem hypertrophic. The number of ALDH1L1+ astrocytes increased significantly in the 5-week cuprizone group compared with the control group. The increase may be due to the proliferation of astrocytes, but there was another possible explanation that under the condition of cuprizone model, increased numbers of astrocytes were counted because hypertrophic morphology enabled them to be more easily identified.

Significant astrogliosis in the corpus callosum, especially the medium corpus callosum, was identified and the astrogliosis might be associated with demyelination. Astrocytes were actively involved in the process of demyelination. It has been shown that astrocytes could phagocytize myelin debris directly [82]. In addition, they were able to recruit microglia to phagocytize myelin debris through the secretion of the chemokine C-X-C motif chemokine Ligand (CXCL) 10 [83].

## **6.2 Other markers of astrocytes**

Apart from GFAP and ALDH1L1, several proteins expressed by astrocytes were taken as markers of astrocytes, e.g., S100 $\beta$ , GLT1, AQP4, Cx43, etc. Each marker had its specific expression characteristics when used to label astrocytes.

S100 $\beta$  is a calcium-binding protein and has been used to label astrocytes for decades. Du et al. investigated the expression of S100 $\beta$  in the CNS and demonstrated the expression of S100 $\beta$  by protoplasmic astrocytes and oligodendrocyte lineage cells [84]. Vives et al. identified the expression of S100 $\beta$  by neurons using transgenic mice [85]. Thus, S100 $\beta$  is not a specific marker of astrocytes.

GLT1 is a kind of glutamate transporter. In a study, Yang et al. suggested that the same astrocyte population expressed GLT1 and ALDH1L1 simultaneously [72]. Nevertheless, GLT1 was found to be expressed by neurons as well [86–88]. In addition, the expression of GLT1 in reactive astrocytes remained in controversy. Some authors proposed a reduction of GLT1 expression in reactive astrocytes [89,90], while a few studies reported an elevated expression of GLT1 by reactive astrocytes [91].

Schreiner et al. demonstrated a pattern with increased expression of GLT1 at the sites of glial scar, yet the expression of GLT1 was reduced at the sites distant from glial scar [92].

AQP4 is a protein with the pivotal function of water exchange, and it is usually described as the predominant water channel in the CNS [93]. The expression of AQP4 exhibited an apparent region-specific property. AQP4 was intensely expressed by astrocytes in cerebellum and in regions in contact with water, e.g., astrocytic end-feet surrounding blood vessels, regions abutting ventricles and subarachnoid space [94]. Besides, ependymal cells [95] and capillary endothelial cells expressed AQP4 as well [96].

Cx43 is a member of connexins which constitute the gap junctions between astrocytes [97]. The astrocytic expression of Cx43 after CNS injury changed with heterogeneity and complexity [98]. Elevated expression of Cx43 was documented in the striatum of mild ischemia damage, while the striatum of severe ischemia damage displayed areas of reduced Cx43 expression in the center and elevated Cx43 immunoreactivity in the peripheral regions [98]. Cx43 was also expressed in other cell population, e.g., monocytes [99], endothelial cells [100], microglia [101], macrophages [102], and lymphocytes [103].

### **6.3 Astrocyte response and function in MS**

The immune system is an indispensable component in the pathogenesis of MS. It has been evidenced that T helper (Th) 1 cells and Th17 cells mediated the inflammatory cascades of MS and EAE [104,105]. Astrocytes were found as active participants in the inflammatory processes in MS as well since they had intimate interactions with immune cells, and played a crucial role in the development of MS.

At the molecular level, in the brain tissue of MS, astrocytes were found to express major histocompatibility (MHC) class I and MHC class II, molecules necessary for antigen presentation [106,107]. Besides, co-stimulatory molecules B7-1 and B7-2 were also demonstrated to be expressed by reactive astrocytes in chronic active lesions of

MS through double immunofluorescent staining [108]. These molecules were necessary components of antigen presenting cells and the expression of these molecules by astrocytes indicated that astrocytes may serve as antigen presenting cells in MS. Astrocytes exhibited such ability not only in MS but also in other neurodegenerative diseases. For example, it has been shown that astrocytes expressing MHC class II and co-stimulatory molecules had close interactions with CD4<sup>+</sup> T cells in Parkinson's disease [109].

In addition, it has been shown that astrocytes produce a variety of cytokines and chemokines, e.g., IL-12 [110], IL-23 [111], IL-27 [112], C-C motif chemokine ligand (CCL) 2 [113], CCL5 [114], CCL20 [115], CXCL1 [116], CXCL10 [117], and CXCL12 [118], to modulate immune responses in MS and the EAE animal models. These cytokines and chemokines could exacerbate or restrain the inflammation in the CNS, and some of them may possess both pro-inflammatory and anti-inflammatory capacity. IL-12 is a cytokine produced by astrocytes and microglia [119]. IL-12 was implicated in the differentiation of naive CD4<sup>+</sup> T cells into Th1 cells [120,121], which were proposed to contribute to the development of MS [122]. Cris et al. demonstrated that astrocytes had the potential to express all subunits of IL-12 in the context of inflammation [123].

IL-23 is a heterodimeric cytokine of IL-12 because IL23 has a same subunit p40 as IL12 and a distinct subunit p19. It has been shown that the subunit p19 of IL23 was produced by astrocytes under the condition of cell stress [123]. Thakker et al. demonstrated that IL-23 played an important role in the pathogenesis of EAE [124], the differentiation of naive CD4<sup>+</sup> T cells into Th17 cells [125], and supporting the survival and expansion of Th17 cells [126]. Moreover, Nitsch et al. demonstrated an elevated B cell accumulation in the EAE model using transgenic mice with targeted expression of IL23 by astrocytes [111].

Up-regulated expression of IL-27 by astrocytes was detected within post-mortem lesions of MS compared with normal brain tissues, and the expression level of IL-27 was elevated in cultured human astrocytes when stimulated with inflammatory cytokines [112]. It has been shown that IL27 could reduce the severity of EAE through



mediating the function of regulatory T cells in animal models [127], and in MS IL-27 exhibited a neuroprotective impact through strengthening the function of regulatory T cells and restraining the function of Th17 cells [128].

CCL2 is a chemokine with the capacity to recruit monocytes, macrophages, T cells, B cells, natural killer cells [129]. The astrocytic expression of CCL2 was confirmed in active white matter lesions [130]. It has been shown that CCL2 knockout from astrocytes resulted in decreased macrophage and T cell infiltration, dampened the activation of astrocytes and microglia, and thus reduced inflammation and demyelination in EAE models [113,131], implying CCL2 could exacerbate inflammatory cascades. He et al. found that the secretion of CCL2 from astrocytes could be induced by TNF- $\alpha$  [132], a pro-inflammatory cytokine.

CCL5, a proinflammatory chemoattractant for immune cells [133], could be produced by astrocytes [114]. The CCL5 level was demonstrated higher in the cerebrospinal fluid (CSF) of relapsing MS patients compared to stable MS patients [134]. Dos et al. investigated the function of CCL5 in the EAE models and proposed that CCL5 had an impact on the adhesion of leukocyte to the brain blood vessels [135].

CCL20 has been shown to facilitate the recruitment of T cells and B cells [136]. Astrocytes were the main producer of CCL20 in the CNS of EAE models [137]. CCL20 concentrations in the serum of MS patients was elevated [138], and plasma level of CCL20 positively correlated to the severity of MS [139]. Reboldi et al. demonstrated that CCL20 induced the trafficking of pathogenic Th17 cells into the CNS via choroid plexus [140].

CXCL1 is a member of the CXCL chemokine family. Omari et al. demonstrated for the first time that the reactive astrocytes secreted CXCL1 in the MS lesion, and in cultured astrocytes it was IL-1 $\beta$  that modulated the production of CXCL1 in astrocytes [141]. It has been shown that astrocyte-derived CXCL1 induced the proliferation of OPCs [142] and hindered the migration of OPCs [143], which were necessary steps for remyelination. And the beneficial effects of improved remyelination were confirmed in EAE models using transgenic mice overexpressing CXCL1 [144]. On the other hand, CXCL1 may aggravate EAE via the recruitment of neutrophils [116]. These conflicting

data revealed the dual functions of CXCL1.

The presence of CXCL10 expression by astrocytes was detected in MS lesions [145]. Sørensen et al. studied the CSF level of CXCL10 in different MS patient cohorts and found that the RRMS group had a prominently increased CSF level of CXCL10 compared with the control group. Furthermore, CXCL10 exhibited the potential to induce the infiltration of C-X-C Motif chemokine Receptor (CXCR) 3 positive T cells [145], or CD4<sup>+</sup> T cells [146], antibodies secreting cells [117] and neutrophils [147] into the brain parenchyma.

CXCL12 could be expressed by reactive astrocytes in MS lesion [118]. The CXCL12 levels in CSF [148] and MS lesion [118] were significantly elevated. It has been shown that the production of CXCL12 in astrocytes was induced by IL-1 $\beta$  and MBP [118]. Coupled with its property of attracting lymphocytes and macrophages into the CNS, CXCL12 was proposed as a neurotoxic molecule by some authors [118,149]. Yet recent studies revealed that CXCL12 could exert diverse neuroprotective effects. For example, CXCL12 boosted the neuronal repair [150], facilitated the differentiation of OPCs [151], converted the Th1 cells into regulatory T cells [152], restrained the migration of immune cells from perivascular space into parenchyma [153], implying CXCL12 may serve as an anti-inflammatory factor.

At the cellular level, astrocytes were found to respond to all CNS insults through a process commonly termed reactive astrogliosis. Hyperplasia and hypertrophy of astrocytes were seen as the typical pathological traits of reactive astrocytes [154]. Reactive astrocytes exhibited morphological changes of hypertrophy, with enlarged cell nuclei, swollen cytoplasm, and decreased process density [155,156].

Reactive astrocytes with hypertrophic morphology were present within acute lesions and at the margin of subacute lesions [82]. Astrocytes in inactive plaques appeared with small somas, nuclei and elongated thin processes, while in the white matter, the arrangement of astrocytes seemed in an isomorphic pattern in agreement with prior tract architecture [156].

Another prominent phenomenon was glial scar formation in the center of chronic inactive lesions [157]. At the rim of a lesion where the microenvironment was less

disturbed, glial scars were absent [158]. Glial scars mainly consisted of reactive astrocytes and chondroitin sulfate proteoglycans expressed by reactive astrocytes. Glial scars were believed to have both beneficial and detrimental effects. On the one hand, Glial scars with compact tissue reorganization may restrict the spread of inflammation [158], on the other hand, glial scars may hinder remyelination as chondroitin sulfate proteoglycans in glial scars impaired oligodendrocyte differentiation [159]. Moreover, chondroitin sulfate proteoglycans were found to strengthen the infiltration of leucocytes in MS [160]. However, a recent study proposed that remyelination was not affected by the glial scar formation in EAE models [161].

It should be noted that the hypertrophic morphology of reactive astrocytes was based on immunostaining for GFAP. The upregulation of GFAP was a prominent feature of reactive astrogliosis and had a profound influence on astrocyte activation [162].

As previously described, two phenotypes of reactive astrocytes were identified, “A1” and “A2”. A1 was found to be a neurotoxic phenotype of reactive astrocytes characterized by upregulation of complement component C3. The presence of A1 astrocytes in MS has been identified. A1 reactive astrocytes has been demonstrated to intimately correlate with CD68<sup>+</sup> activated microglia/macrophages in MS lesions, implying that astrocytes may be a potential driver of MS development [56]. A2 reactive astrocytes promoting survival of neurons and synapse repair were induced in an ischemic animal model [163]. These astrocytes with distinct functions indicated they may exert proinflammatory functions or anti-inflammatory functions in a microenvironment dependent manner. Given the temporally and spatially complex pathology, these astrocytes with distinct properties may exist in different regions simultaneously or appear in the same region during different phases [164].

## **6.4 The function of ALDH1L1 in CNS.**

ALDH1L1 is a folate metabolic enzyme. Studies have shown ALDH1L1 may be a candidate tumor suppressor as accelerated tumor growth was found in ALDH1L1 knockout mice [165], and the relation of poor prognosis of tumor patients to low

expression of ALDH1L1 was identified [166].

There were a few studies investigated the expression of ALDH1L1 in the CNS. The expression of ALDH1L1 in the spinal cord during its development was reduced, while upregulated expression of ALDH1L1 in reactive astrocytes was identified in acute brain injury and chronic neurodegenerative diseases [72], including MS [156] and Alzheimer disease [167]. In the cuprizone models of MS, Castillo et al. found elevated expression levels of ALDH1L1 messenger ribonucleic acid (mRNA) to the same extent in all brain regions and reduced ALDH1L1 mRNA expression levels during the remyelination process [168].

The specific function of ALDH1L1 in the CNS and its influence on CNS diseases remain poorly understood. Williams et al. proposed that ALDH1L1 may correlate with human neural tube defects as they found the expression of ALDH1L1 was centralized to the midline of the neural tube during early murine brain development. Moreover, ALDH1L1 was associated with ischemic stroke by a genome-wide Meta-Analysis [169].

## 7. Conclusion

This study revealed that a proportion of cortical astrocytes reduced the expression of ALDH1L1 in a region-dependent manner. In MS, the expression of ALDH1L1 by some astrocytes seemed centralized to the somas of astrocytes. In the cuprizone models, significant astrogliosis in the medial part of the corpus callosum was found by anti-ALDH1L1 immunohistochemistry. In summary, these data suggested a dynamic regulation of ALDH1L1 in both the healthy and diseased CNS.

Overall, this study supports ALDH1L1 as a marker used to visualize astrocytes in the cortex and white matter. The regional expression loss of ALDH1L1 by astrocytes, the underlying mechanism, and potential function alteration need further investigation.

## 8. List of figures

Figure 1: Schematic of MS pathogenesis hypothesis. ....	10
Figure 2: Image of a single protoplasmic astrocyte. ....	14
Figure 3: Schematic of complex function of astrocytes. ....	15
Figure 4: Schematic of astrogliosis. ....	16
Figure 5: Schematic of astrocytes with weak anti-ALDH1L1 staining intensity. ....	19
Figure 6: Schematic of immunohistochemical staining with ABC method. ....	24
Figure 7: Schematic of double immunofluorescent staining. ....	29
Figure 8: Schematic of negative controls in double immunofluorescent staining. ....	32
Figure 9: Schematic of ROIs. ....	36
Figure 10: Astrocytes visualized by immunohistochemical staining for ALDH1L1. ....	38
Figure 11: ALDH1L1 expression in human brain cortex. ....	40
Figure 12: Anti-ALDH1L1 staining intensity in the human brain cortex. ....	41
Figure 13: GFAP expression in human brain cortex. ....	42
Figure 14: Astrocytes in mouse brain cortex. ....	43
Figure 15: Cellular areas of murine astrocytes. ....	45
Figure 16: Image of consecutive sections stained for ALDH1L1, GFAP, and Laminin. ....	46
Figure 17: Image of double immunofluorescent staining for ALDH1L1 and CD31. ....	48
Figure 18: Image of astrocytes in control human and MS brain tissues. ....	49
Figure 19: Image of astrocytes in the cortex of cuprizone models. ....	50
Figure 20: Astrogliosis in the medium corpus callosum of cuprizone models. ....	51
Figure 21: Schematic of negative controls. ....	52

\*Figure 1, 3, 4, 6, 7, 8 were created with Biorender.com.

## 9. List of tables

Table 1: Preparation of perfusion solution .....	21
Table 2: Tissue dehydration in Histokinette .....	22
Table 3: Deparaffinization and rehydration .....	25
Table 4: Primary antibodies applied for immunohistochemical staining .....	26
Table 5: Secondary antibodies applied for immunohistochemical staining .....	27
Table 6: Dehydration .....	27
Table 7: Protocol of immunohistochemical staining .....	28
Table 8: Primary antibodies used for immunofluorescent staining .....	30
Table 9: Secondary antibodies used for immunofluorescent staining .....	31
Table 10: Protocol of double immunofluorescent staining .....	31
Table 11: Quantification of staining intensity .....	35
Table 12: Cellular areas of astrocytes .....	44
Table 13: List of chemicals .....	77
Table 14: List of solutions .....	78

## 10. References

1. Walton, C.; King, R.; Rechtman, L.; Kaye, W.; Leray, E.; Marrie, R.A.; Robertson, N.; La Rocca, N.; Uitdehaag, B.; van der Mei, I.; et al. Rising prevalence of multiple sclerosis worldwide: Insights from the Atlas of MS, third edition. *Mult. Scler.* **2020**, *26*, 1816–1821, doi:10.1177/1352458520970841.
2. Harbo, H.F.; Gold, R.; Tintoré, M. Sex and gender issues in multiple sclerosis. *Ther. Adv. Neurol. Disord.* **2013**, *6*, 237–248, doi:10.1177/1756285613488434.
3. Wallin, M.T.; Culpepper, W.J.; Campbell, J.D.; Nelson, L.M.; Langer-Gould, A.; Marrie, R.A.; Cutter, G.R.; Kaye, W.E.; Wagner, L.; Tremlett, H.; et al. The prevalence of MS in the United States: A population-based estimate using health claims data. *Neurology* **2019**, *92*, e1029–e1040, doi:10.1212/WNL.0000000000007035.
4. McDowell, T.-Y.; Amr, S.; Culpepper, W.J.; Langenberg, P.; Royal, W.; Bever, C.; Bradham, D.D. Sun exposure, vitamin D and age at disease onset in relapsing multiple sclerosis. *Neuroepidemiology* **2011**, *36*, 39–45, doi:10.1159/000322512.
5. Ostkamp, P.; Salmen, A.; Pignolet, B.; Görlich, D.; Andlauer, T.F.M.; Schulte-Mecklenbeck, A.; Gonzalez-Escamilla, G.; Bucciarelli, F.; Gennero, I.; Breuer, J.; et al. Sunlight exposure exerts immunomodulatory effects to reduce multiple sclerosis severity. *Proc. Natl. Acad. Sci. U. S. A.* **2021**, *118*, doi:10.1073/pnas.2018457118.
6. Bjornevik, K.; Cortese, M.; Healy, B.C.; Kuhle, J.; Mina, M.J.; Leng, Y.; Elledge, S.J.; Niebuhr, D.W.; Scher, A.I.; Munger, K.L.; et al. Longitudinal analysis reveals high prevalence of Epstein-Barr virus associated with multiple sclerosis. *Science* **2022**, *375*, 296–301, doi:10.1126/science.abj8222.
7. Lanz, T.V.; Brewer, R.C.; Ho, P.P.; Moon, J.-S.; Jude, K.M.; Fernandez, D.; Fernandes, R.A.; Gomez, A.M.; Nadj, G.-S.; Bartley, C.M.; et al. Clonally expanded B cells in multiple sclerosis bind EBV EBNA1 and GlialCAM. *Nature* **2022**, *603*, 321–327, doi:10.1038/s41586-022-04432-7.
8. Lomakin, Y.; Arapidi, G.P.; Chernov, A.; Ziganshin, R.; Tcyganov, E.; Lyadova, I.; Butenko, I.O.; Osetrova, M.; Ponomarenko, N.; Telegin, G.; et al. Exposure to the Epstein-Barr Viral Antigen Latent Membrane Protein 1 Induces Myelin-Reactive Antibodies In Vivo. *Front. Immunol.* **2017**, *8*, 777, doi:10.3389/fimmu.2017.00777.
9. Mumford, C.J.; Wood, N.W.; Kellar-Wood, H.; Thorpe, J.W.; Miller, D.H.; Compston, D.A. The British Isles survey of multiple sclerosis in twins. *Neurology* **1994**, *44*, 11–15, doi:10.1212/wnl.44.1.11.
10. Eskandarieh, S.; Heydarpour, P.; Minagar, A.; Pourmand, S.; Sahraian, M.A. Multiple Sclerosis Epidemiology in East Asia, South East Asia and South Asia: A Systematic Review. *Neuroepidemiology* **2016**, *46*, 209–221, doi:10.1159/000444019.
11. Heydarpour, P.; Khoshkish, S.; Abtahi, S.; Moradi-Lakeh, M.; Sahraian, M.A. Multiple Sclerosis Epidemiology in Middle East and North Africa: A Systematic Review and Meta-Analysis. *Neuroepidemiology* **2015**, *44*, 232–244, doi:10.1159/000431042.
12. Lincoln, M.R.; Montpetit, A.; Cader, M.Z.; Saarela, J.; Dymment, D.A.; Tiislar, M.; Ferretti, V.; Tienari, P.J.; Sadovnick, A.D.; Peltonen, L.; et al. A predominant role for the HLA class II



- region in the association of the MHC region with multiple sclerosis. *Nat. Genet.* **2005**, *37*, 1108–1112, doi:10.1038/ng1647.
13. Didonna, A.; Oksenberg, J.R. Genetic determinants of risk and progression in multiple sclerosis. *Clin. Chim. Acta* **2015**, *449*, 16–22, doi:10.1016/j.cca.2015.01.034.
  14. Kipp, M.; van der Valk, P.; Amor, S. Pathology of multiple sclerosis. *CNS Neurol. Disord. Drug Targets* **2012**, *11*, 506–517, doi:10.2174/187152712801661248.
  15. Bø, L.; Vedeler, C.A.; Nyland, H.I.; Trapp, B.D.; Mørk, S.J. Subpial demyelination in the cerebral cortex of multiple sclerosis patients. *J. Neuropathol. Exp. Neurol.* **2003**, *62*, 723–732, doi:10.1093/jnen/62.7.723.
  16. Ghasemi, N.; Razavi, S.; Nikzad, E. Multiple Sclerosis: Pathogenesis, Symptoms, Diagnoses and Cell-Based Therapy. *Cell J.* **2017**, *19*, 1–10, doi:10.22074/cellj.2016.4867.
  17. McKay, K.A.; Kwan, V.; Duggan, T.; Tremlett, H. Risk factors associated with the onset of relapsing-remitting and primary progressive multiple sclerosis: a systematic review. *Biomed Res. Int.* **2015**, *2015*, 817238, doi:10.1155/2015/817238.
  18. Giovannoni, G. Management of secondary-progressive multiple sclerosis. *CNS Drugs* **2004**, *18*, 653–669, doi:10.2165/00023210-200418100-00003.
  19. Leary, S.M.; Thompson, A.J. Primary progressive multiple sclerosis : current and future treatment options. *CNS Drugs* **2005**, *19*, 369–376, doi:10.2165/00023210-200519050-00001.
  20. Reynders, T.; D'haeseleer, M.; Keyser, J. de; Nagels, G.; D'hooghe, M.B. Definition, prevalence and predictive factors of benign multiple sclerosis. *eNeurologicalSci* **2017**, *7*, 37–43, doi:10.1016/j.ensci.2017.05.002.
  21. Hampshire-Araújo, F.; Bergmann, A.; Alvarenga, R.M.P.; Vasconcelos, C.C.F. Malignant multiple sclerosis: clinical and demographic prognostic factors. *Arq. Neuropsiquiatr.* **2017**, *75*, 139–141, doi:10.1590/0004-282X20170010.
  22. Titus, H.E.; Chen, Y.; Podojil, J.R.; Robinson, A.P.; Balabanov, R.; Popko, B.; Miller, S.D. Pre-clinical and Clinical Implications of "Inside-Out" vs. "Outside-In" Paradigms in Multiple Sclerosis Etiopathogenesis. *Front. Cell. Neurosci.* **2020**, *14*, 599717, doi:10.3389/fncel.2020.599717.
  23. Sen, M.K.; Almuslehi, M.S.M.; Shortland, P.J.; Coorsen, J.R.; Mahns, D.A. Revisiting the Pathoetiology of Multiple Sclerosis: Has the Tail Been Wagging the Mouse? *Front. Immunol.* **2020**, *11*, 572186, doi:10.3389/fimmu.2020.572186.
  24. Shin, T.; Ahn, M.; Matsumoto, Y. Mechanism of experimental autoimmune encephalomyelitis in Lewis rats: recent insights from macrophages. *Anat. Cell Biol.* **2012**, *45*, 141–148, doi:10.5115/acb.2012.45.3.141.
  25. Kim, S.; Lee, Y.-I.; Chang, K.-Y.; Lee, D.-W.; Cho, S.C.; Ha, Y.W.; Na, J.E.; Im Rhyu, J.; Park, S.C.; Park, H.-C. Promotion of Remyelination by Sulfasalazine in a Transgenic Zebrafish Model of Demyelination. *Mol. Cells* **2015**, *38*, 1013–1021, doi:10.14348/molcells.2015.0246.
  26. Chen, G.Q.; Chen, Y.Y.; Wang, X.S.; Wu, S.Z.; Yang, H.M.; Xu, H.Q.; He, J.C.; Wang, X.T.; Chen, J.F.; Zheng, R.Y. Chronic caffeine treatment attenuates experimental autoimmune encephalomyelitis induced by guinea pig spinal cord homogenates in Wistar rats. *Brain Research* **2010**, *1309*, 116–125, doi:10.1016/j.brainres.2009.10.054.
  27. Williams, R.M.; Lees, M.B.; Cambi, F.; Macklin, W.B. Chronic experimental allergic

- encephalomyelitis induced in rabbits with bovine white matter proteolipid apoprotein. *J. Neuropathol. Exp. Neurol.* **1982**, *41*, 508–521, doi:10.1097/00005072-198209000-00004.
28. Stimmer, L.; Fovet, C.-M.; Serguera, C. Experimental Models of Autoimmune Demyelinating Diseases in Nonhuman Primates. *Vet. Pathol.* **2018**, *55*, 27–41, doi:10.1177/0300985817712794.
  29. Kipp, M.; Nyamoya, S.; Hochstrasser, T.; Amor, S. Multiple sclerosis animal models: a clinical and histopathological perspective. *Brain Pathol.* **2017**, *27*, 123–137, doi:10.1111/bpa.12454.
  30. Miller, S.D.; Karpus, W.J. Experimental autoimmune encephalomyelitis in the mouse. *Curr. Protoc. Immunol.* **2007**, *Chapter 15*, Unit 15.1, doi:10.1002/0471142735.im1501s77.
  31. Mokhtarian, F.; McFarlin, D.E.; Raine, C.S. Adoptive transfer of myelin basic protein-sensitized T cells produces chronic relapsing demyelinating disease in mice. *Nature* **1984**, *309*, 356–358, doi:10.1038/309356a0.
  32. Goverman, J.; Woods, A.; Larson, L.; Weiner, L.P.; Hood, L.; Zaller, D.M. Transgenic mice that express a myelin basic protein-specific T cell receptor develop spontaneous autoimmunity. *Cell* **1993**, *72*, 551–560, doi:10.1016/0092-8674(93)90074-Z.
  33. Lando, Z.; Teitelbaum, D.; Arnon, R. Effect of cyclophosphamide on suppressor cell activity in mice unresponsive to EAE. *J. Immunol.* **1979**, *123*, 2156–2160.
  34. Bittner, S.; Afzali, A.M.; Wiendl, H.; Meuth, S.G. Myelin oligodendrocyte glycoprotein (MOG35-55) induced experimental autoimmune encephalomyelitis (EAE) in C57BL/6 mice. *J. Vis. Exp.* **2014**, doi:10.3791/51275.
  35. Wootla, B.; Denic, A.; Keegan, B.M.; Winters, J.L.; Astapenko, D.; Warrington, A.E.; Bieber, A.J.; Rodriguez, M. Evidence for the role of B cells and immunoglobulins in the pathogenesis of multiple sclerosis. *Neurol. Res. Int.* **2011**, *2011*, 780712, doi:10.1155/2011/780712.
  36. Bebo, B.F.; Vandenberg, A.A.; Offner, H. Male SJL mice do not relapse after induction of EAE with PLP 139-151. *J. Neurosci. Res.* **1996**, *45*, 680–689, doi:10.1002/(SICI)1097-4547(19960915)45:6<680:AID-JNR4>3.0.CO;2-4.
  37. McRae, B.L.; Kennedy, M.K.; Tan, L.-J.; Dal Canto, M.C.; Picha, K.S.; Miller, S.D. Induction of active and adoptive relapsing experimental autoimmune encephalomyelitis (EAE) using an encephalitogenic epitope of proteolipid protein. *Journal of Neuroimmunology* **1992**, *38*, 229–240, doi:10.1016/0165-5728(92)90016-E.
  38. Mony, J.T.; Khorooshi, R.; Owens, T. MOG extracellular domain (p1-125) triggers elevated frequency of CXCR3+ CD4+ Th1 cells in the CNS of mice and induces greater incidence of severe EAE. *Mult. Scler.* **2014**, *20*, 1312–1321, doi:10.1177/1352458514524086.
  39. Mori, Y.; Murakami, M.; Arima, Y.; Zhu, D.; Terayama, Y.; Komai, Y.; Nakatsuji, Y.; Kamimura, D.; Yoshioka, Y. Early pathological alterations of lower lumbar cords detected by ultrahigh-field MRI in a mouse multiple sclerosis model. *Int. Immunol.* **2014**, *26*, 93–101, doi:10.1093/intimm/dxt044.
  40. Lee, H.-G.; Lee, J.-U.; Kim, D.-H.; Lim, S.; Kang, I.; Choi, J.-M. Pathogenic function of bystander-activated memory-like CD4+ T cells in autoimmune encephalomyelitis. *Nat. Commun.* **2019**, *10*, 709, doi:10.1038/s41467-019-08482-w.
  41. van Langelaar, J.; Rijvers, L.; Smolders, J.; van Luijn, M.M. B and T Cells Driving Multiple Sclerosis: Identity, Mechanisms and Potential Triggers. *Front. Immunol.* **2020**, *11*, 760,

doi:10.3389/fimmu.2020.00760.

42. McFadden, K.; Wiley, C.A. The Pathology of Multiple Sclerosis Is Location-Dependent: No Significant Complement Activation Is Detected in Purely Cortical Lesions. *Yearbook of Pathology and Laboratory Medicine* **2007**, *2007*, 229–230, doi:10.1016/S1077-9108(08)70400-6.
43. McMahon, E.J.; Suzuki, K.; Matsushima, G.K. Peripheral macrophage recruitment in cuprizone-induced CNS demyelination despite an intact blood–brain barrier. *Journal of Neuroimmunology* **2002**, *130*, 32–45, doi:10.1016/S0165-5728(02)00205-9.
44. Hillis, J.M.; Davies, J.; Mundim, M.V.; Al-Dalahmah, O.; Szele, F.G. Cuprizone demyelination induces a unique inflammatory response in the subventricular zone. *J. Neuroinflammation* **2016**, *13*, 190, doi:10.1186/s12974-016-0651-2.
45. Berghoff, S.A.; Düking, T.; Spieth, L.; Winchenbach, J.; Stumpf, S.K.; Gerndt, N.; Kusch, K.; Ruhwedel, T.; Möbius, W.; Saher, G. Blood-brain barrier hyperpermeability precedes demyelination in the cuprizone model. *Acta Neuropathol. Commun.* **2017**, *5*, 94, doi:10.1186/s40478-017-0497-6.
46. Kaddatz, H.; Joost, S.; Nedelcu, J.; Chrzanowski, U.; Schmitz, C.; Gingele, S.; Gudi, V.; Stangel, M.; Zhan, J.; Santrau, E.; et al. Cuprizone-induced demyelination triggers a CD8-pronounced T cell recruitment. *Glia* **2021**, *69*, 925–942, doi:10.1002/glia.23937.
47. Zhan, J.; Mann, T.; Joost, S.; Behrang, N.; Frank, M.; Kipp, M. The Cuprizone Model: Dos and Do Nots. *Cells* **2020**, *9*, doi:10.3390/cells9040843.
48. Goldberg, J.; Clarner, T.; Beyer, C.; Kipp, M. Anatomical Distribution of Cuprizone-Induced Lesions in C57BL6 Mice. *J. Mol. Neurosci.* **2015**, *57*, 166–175, doi:10.1007/s12031-015-0595-5.
49. Verkhratsky, A.; Nedergaard, M. Physiology of Astroglia. *Physiol. Rev.* **2018**, *98*, 239–389, doi:10.1152/physrev.00042.2016.
50. Ricci, G.; Volpi, L.; Pasquali, L.; Petrozzi, L.; Siciliano, G. Astrocyte-neuron interactions in neurological disorders. *J. Biol. Phys.* **2009**, *35*, 317–336, doi:10.1007/s10867-009-9157-9.
51. Chung, W.-S.; Allen, N.J.; Eroglu, C. Astrocytes Control Synapse Formation, Function, and Elimination. *Cold Spring Harb. Perspect. Biol.* **2015**, *7*, a020370, doi:10.1101/cshperspect.a020370.
52. Andersen, J.V.; Markussen, K.H.; Jakobsen, E.; Schousboe, A.; Waagepetersen, H.S.; Rosenberg, P.A.; Aldana, B.I. Glutamate metabolism and recycling at the excitatory synapse in health and neurodegeneration. *Neuropharmacology* **2021**, *196*, 108719, doi:10.1016/j.neuropharm.2021.108719.
53. Walz, W. Role of astrocytes in the clearance of excess extracellular potassium. *Neurochem. Int.* **2000**, *36*, 291–300, doi:10.1016/S0197-0186(99)00137-0.
54. Szu, J.I.; Binder, D.K. The Role of Astrocytic Aquaporin-4 in Synaptic Plasticity and Learning and Memory. *Front. Integr. Neurosci.* **2016**, *10*, 8, doi:10.3389/fnint.2016.00008.
55. Giaume, C.; McCarthy, K.D. Control of gap-junctional communication in astrocytic networks. *Trends Neurosci.* **1996**, *19*, 319–325, doi:10.1016/0166-2236(96)10046-1.
56. Liddel, S.A.; Guttenplan, K.A.; Clarke, L.E.; Bennett, F.C.; Bohlen, C.J.; Schirmer, L.; Bennett, M.L.; Münch, A.E.; Chung, W.-S.; Peterson, T.C.; et al. Neurotoxic reactive astrocytes are induced by activated microglia. *Nature* **2017**, *541*, 481–487,

doi:10.1038/nature21029.

57. Frei, K.; Nohava, K.; Malipiero, U.V.; Schwerdel, C.; Fontana, A. Production of macrophage colony-stimulating factor by astrocytes and brain macrophages. *Journal of Neuroimmunology* **1992**, *40*, 189–195, doi:10.1016/0165-5728(92)90133-6.
58. Hammond, T.R.; Gadea, A.; Dupree, J.; Kerninon, C.; Nait-Oumesmar, B.; Aguirre, A.; Gallo, V. Astrocyte-derived endothelin-1 inhibits remyelination through notch activation. *Neuron* **2014**, *81*, 588–602, doi:10.1016/j.neuron.2013.11.015.
59. Niu, J.; Tsai, H.-H.; Hoi, K.K.; Huang, N.; Yu, G.; Kim, K.; Baranzini, S.E.; Xiao, L.; Chan, J.R.; Fancy, S.P.J. Aberrant oligodendroglial-vascular interactions disrupt the blood-brain barrier, triggering CNS inflammation. *Nat. Neurosci.* **2019**, *22*, 709–718, doi:10.1038/s41593-019-0369-4.
60. Sofroniew, M.V.; Vinters, H.V. Astrocytes: biology and pathology. *Acta Neuropathol.* **2010**, *119*, 7–35, doi:10.1007/s00401-009-0619-8.
61. Falcone, C.; Penna, E.; Hong, T.; Tarantal, A.F.; Hof, P.R.; Hopkins, W.D.; Sherwood, C.C.; Noctor, S.C.; Martínez-Cerdeño, V. Cortical Interlaminar Astrocytes Are Generated Prenatally, Mature Postnatally, and Express Unique Markers in Human and Nonhuman Primates. *Cereb. Cortex* **2021**, *31*, 379–395, doi:10.1093/cercor/bhaa231.
62. Verkhratsky, A.; Bush, N.; Nedergaard, M.; Butt, A. The Special Case of Human Astrocytes. *Neuroglia* **2018**, *1*, 21–29, doi:10.3390/neuroglia1010004.
63. Falcone, C.; McBride, E.L.; Hopkins, W.D.; Hof, P.R.; Manger, P.R.; Sherwood, C.C.; Noctor, S.C.; Martínez-Cerdeño, V. Redefining varicose projection astrocytes in primates. *Glia* **2022**, *70*, 145–154, doi:10.1002/glia.24093.
64. Colombo, J.A.; Reisin, H.D. Interlaminar astroglia of the cerebral cortex: a marker of the primate brain. *Brain Research* **2004**, *1006*, 126–131, doi:10.1016/j.brainres.2004.02.003.
65. Yamada, K.; Watanabe, M. Cytodifferentiation of Bergmann glia and its relationship with Purkinje cells. *Anat. Sci. Int.* **2002**, *77*, 94–108, doi:10.1046/j.0022-7722.2002.00021.x.
66. Trentin, A.G. Thyroid hormone and astrocyte morphogenesis. *J. Endocrinol.* **2006**, *189*, 189–197, doi:10.1677/joe.1.06680.
67. Matyash, V.; Kettenmann, H. Heterogeneity in astrocyte morphology and physiology. *Brain Res. Rev.* **2010**, *63*, 2–10, doi:10.1016/j.brainresrev.2009.12.001.
68. Cahoy, J.D.; Emery, B.; Kaushal, A.; Foo, L.C.; Zamanian, J.L.; Christopherson, K.S.; Xing, Y.; Lubischer, J.L.; Krieg, P.A.; Krupenko, S.A.; et al. A transcriptome database for astrocytes, neurons, and oligodendrocytes: a new resource for understanding brain development and function. *J. Neurosci.* **2008**, *28*, 264–278, doi:10.1523/JNEUROSCI.4178-07.2008.
69. Wilhelmsson, U.; Bushong, E.A.; Price, D.L.; Smarr, B.L.; van Phung; Terada, M.; Ellisman, M.H.; Pekny, M. Redefining the concept of reactive astrocytes as cells that remain within their unique domains upon reaction to injury. *Proc. Natl. Acad. Sci. U. S. A.* **2006**, *103*, 17513–17518, doi:10.1073/pnas.0602841103.
70. Casper, K.B.; McCarthy, K.D. GFAP-positive progenitor cells produce neurons and oligodendrocytes throughout the CNS. *Mol. Cell. Neurosci.* **2006**, *31*, 676–684, doi:10.1016/j.mcn.2005.12.006.
71. Zamanian, J.L.; Xu, L.; Foo, L.C.; Nouri, N.; Zhou, L.; Giffard, R.G.; Barres, B.A. Genomic analysis of reactive astrogliosis. *J. Neurosci.* **2012**, *32*, 6391–6410,

- doi:10.1523/JNEUROSCI.6221-11.2012.
72. Yang, Y.; Vidensky, S.; Jin, L.; Jie, C.; Lorenzini, I.; Frankl, M.; Rothstein, J.D. Molecular comparison of GLT1+ and ALDH1L1+ astrocytes in vivo in astroglial reporter mice. *Glia* **2011**, *59*, 200–207, doi:10.1002/glia.21089.
  73. Foo, L.C.; Dougherty, J.D. Aldh1L1 is expressed by postnatal neural stem cells in vivo. *Glia* **2013**, *61*, 1533–1541, doi:10.1002/glia.22539.
  74. High Resolution Mouse Brain Atlas. Available online: <http://www.hms.harvard.edu/research/brain/atlas.html> (accessed on 2 March 2022).
  75. Arnao, M.B.; Acosta, M.; del Rio, J.A.; Varón, R.; García-Cánovas, F. A kinetic study on the suicide inactivation of peroxidase by hydrogen peroxide. *Biochimica et Biophysica Acta (BBA) - Protein Structure and Molecular Enzymology* **1990**, *1041*, 43–47, doi:10.1016/0167-4838(90)90120-5.
  76. Arnao, M.B.; Acosta, M.; del Rio, J.A.; García-Cánovas, F. Inactivation of peroxidase by hydrogen peroxide and its protection by a reductant agent. *Biochimica et Biophysica Acta (BBA) - Protein Structure and Molecular Enzymology* **1990**, *1038*, 85–89, doi:10.1016/0167-4838(90)90014-7.
  77. Bushong, E.A.; Martone, M.E.; Jones, Y.Z.; Ellisman, M.H. Protoplasmic Astrocytes in CA1 Stratum Radiatum Occupy Separate Anatomical Domains. *J. Neurosci.* **2002**, *22*, 183–192, doi:10.1523/JNEUROSCI.22-01-00183.2002.
  78. Oberheim, N.A.; Takano, T.; Han, X.; He, W.; Lin, J.H.C.; Wang, F.; Xu, Q.; Wyatt, J.D.; Pilcher, W.; Ojemann, J.G.; et al. Uniquely hominid features of adult human astrocytes. *J. Neurosci.* **2009**, *29*, 3276–3287, doi:10.1523/JNEUROSCI.4707-08.2009.
  79. Grosche, A.; Grosche, J.; Tackenberg, M.; Scheller, D.; Gerstner, G.; Gumprecht, A.; Pannicke, T.; Hirrlinger, P.G.; Wilhelmsson, U.; Hüttmann, K.; et al. Versatile and simple approach to determine astrocyte territories in mouse neocortex and hippocampus. *PLoS One* **2013**, *8*, e69143, doi:10.1371/journal.pone.0069143.
  80. Behrangi, N.; Lorenz, P.; Kipp, M. Oligodendrocyte Lineage Marker Expression in eGFP-GFAP Transgenic Mice. *J. Mol. Neurosci.* **2020**, doi:10.1007/s12031-020-01771-w.
  81. Liedtke, W.; Edelmann, W.; Bieri, P.L.; Chiu, F.-C.; Cowan, N.J.; Kucherlapati, R.; Raine, C.S. GFAP Is Necessary for the Integrity of CNS White Matter Architecture and Long-Term Maintenance of Myelination. *Neuron* **1996**, *17*, 607–615, doi:10.1016/S0896-6273(00)80194-4.
  82. Ponath, G.; Ramanan, S.; Mubarak, M.; Housley, W.; Lee, S.; Sahinkaya, F.R.; Vortmeyer, A.; Raine, C.S.; Pitt, D. Myelin phagocytosis by astrocytes after myelin damage promotes lesion pathology. *Brain* **2017**, *140*, 399–413, doi:10.1093/brain/aww298.
  83. Skripuletz, T.; Hackstette, D.; Bauer, K.; Gudi, V.; Pul, R.; Voss, E.; Berger, K.; Kipp, M.; Baumgärtner, W.; Stangel, M. Astrocytes regulate myelin clearance through recruitment of microglia during cuprizone-induced demyelination. *Brain* **2013**, *136*, 147–167, doi:10.1093/brain/aws262.
  84. Du, J.; Yi, M.; Zhou, F.; He, W.; Yang, A.; Qiu, M.; Huang, H. S100B is selectively expressed by gray matter protoplasmic astrocytes and myelinating oligodendrocytes in the developing CNS. *Mol. Brain* **2021**, *14*, 154, doi:10.1186/s13041-021-00865-9.
  85. Vives, V.; Alonso, G.; Solal, A.C.; Joubert, D.; Legraverend, C. Visualization of S100B-positive neurons and glia in the central nervous system of EGFP transgenic mice. *J. Comp.*

- Neurol.* **2003**, *457*, 404–419, doi:10.1002/cne.10552.
86. Martin, L.J.; Brambrink, A.M.; Lehmann, C.; Portera-Cailliau, C.; Koehler, R.; Rothstein, J.; Traystman, R.J. Hypoxia-ischemia causes abnormalities in glutamate transporters and death of astroglia and neurons in newborn striatum. *Ann. Neurol.* **1997**, *42*, 335–348, doi:10.1002/ana.410420310.
  87. Chen, W.; Mahadomrongkul, V.; Berger, U.V.; Bassan, M.; DeSilva, T.; Tanaka, K.; Irwin, N.; Aoki, C.; Rosenberg, P.A. The glutamate transporter GLT1a is expressed in excitatory axon terminals of mature hippocampal neurons. *J. Neurosci.* **2004**, *24*, 1136–1148, doi:10.1523/JNEUROSCI.1586-03.2004.
  88. Mennerick, S.; Dhond, R.P.; Benz, A.; Xu, W.; Rothstein, J.D.; Danbolt, N.C.; Isenberg, K.E.; Zorumski, C.F. Neuronal Expression of the Glutamate Transporter GLT-1 in Hippocampal Microcultures. *J. Neurosci.* **1998**, *18*, 4490–4499, doi:10.1523/JNEUROSCI.18-12-04490.1998.
  89. van Landeghem, F.K.H.; Weiss, T.; Oehmichen, M.; Deimling, A. von. Decreased expression of glutamate transporters in astrocytes after human traumatic brain injury. *J. Neurotrauma* **2006**, *23*, 1518–1528, doi:10.1089/neu.2006.23.1518.
  90. Ginsberg, S.D.; Martin, L.J.; Rothstein, J.D. Regional deafferentation down-regulates subtypes of glutamate transporter proteins. *J. Neurochem.* **1995**, *65*, 2800–2803, doi:10.1046/j.1471-4159.1995.65062800.x.
  91. Kobayashi, E.; Nakano, M.; Kubota, K.; Himuro, N.; Mizoguchi, S.; Chikenji, T.; Otani, M.; Mizue, Y.; Nagaiishi, K.; Fujimiya, M. Activated forms of astrocytes with higher GLT-1 expression are associated with cognitive normal subjects with Alzheimer pathology in human brain. *Sci. Rep.* **2018**, *8*, 1712, doi:10.1038/s41598-018-19442-7.
  92. Schreiner, A.E.; Berlinger, E.; Langer, J.; Kafitz, K.W.; Rose, C.R. Lesion-induced alterations in astrocyte glutamate transporter expression and function in the hippocampus. *ISRN Neurol.* **2013**, *2013*, 893605, doi:10.1155/2013/893605.
  93. Papadopoulos, M.C.; Verkman, A.S. Aquaporin water channels in the nervous system. *Nat. Rev. Neurosci.* **2013**, *14*, 265–277, doi:10.1038/nrn3468.
  94. Hubbard, J.A.; Hsu, M.S.; Seldin, M.M.; Binder, D.K. Expression of the Astrocyte Water Channel Aquaporin-4 in the Mouse Brain. *ASN Neuro* **2015**, *7*, doi:10.1177/1759091415605486.
  95. Castañeyra-Ruiz, L.; González-Marrero, I.; González-Toledo, J.M.; Castañeyra-Ruiz, A.; Paz-Carmona, H. de; Castañeyra-Perdomo, A.; Carmona-Calero, E.M. Aquaporin-4 expression in the cerebrospinal fluid in congenital human hydrocephalus. *Fluids Barriers CNS* **2013**, *10*, 18, doi:10.1186/2045-8118-10-18.
  96. Zhang, C.; Chen, J.; Lu, H. Expression of aquaporin-4 and pathological characteristics of brain injury in a rat model of traumatic brain injury. *Mol. Med. Rep.* **2015**, *12*, 7351–7357, doi:10.3892/mmr.2015.4372.
  97. Nakase, T.; Fushiki, S.; Naus, C.C.G. Astrocytic gap junctions composed of connexin 43 reduce apoptotic neuronal damage in cerebral ischemia. *Stroke* **2003**, *34*, 1987–1993, doi:10.1161/01.STR.0000079814.72027.34.
  98. Hossain, M.Z.; Peeling, J.; Sutherland, G.R.; Hertzberg, E.L.; Nagy, J.I. Ischemia-induced cellular redistribution of the astrocytic gap junctional protein connexin43 in rat brain. *Brain Research* **1994**, *652*, 311–322, doi:10.1016/0006-8993(94)90242-9.

99. Ji, H.; Qiu, R.; Gao, X.; Zhang, R.; Li, X.; Hei, Z.; Yuan, D. Propofol attenuates monocyte-endothelial adhesion via modulating connexin43 expression in monocytes. *Life Sci.* **2019**, *232*, 116624, doi:10.1016/j.lfs.2019.116624.
100. Yuan, D.; Sun, G.; Zhang, R.; Luo, C.; Ge, M.; Luo, G.; Hei, Z. Connexin 43 expressed in endothelial cells modulates monocyte-endothelial adhesion by regulating cell adhesion proteins. *Mol. Med. Rep.* **2015**, *12*, 7146–7152, doi:10.3892/mmr.2015.4273.
101. Eugenin, E.A.; Eckardt, D.; Theis, M.; Willecke, K.; Bennett, M.V.; Saez, J.C. Microglia at brain stab wounds express connexin 43 and in vitro form functional gap junctions after treatment with interferon-gamma and tumor necrosis factor-alpha. *Proc. Natl. Acad. Sci. U.S.A.* **2001**, *98*, 4190–4195, doi:10.1073/pnas.051634298.
102. Rodjakovic, D.; Salm, L.; Beldi, G. Function of Connexin-43 in Macrophages. *Int. J. Mol. Sci.* **2021**, *22*, doi:10.3390/ijms22031412.
103. Oviedo-Orta, E.; Howard Evans, W. Gap junctions and connexin-mediated communication in the immune system. *Biochim. Biophys. Acta* **2004**, *1662*, 102–112, doi:10.1016/j.bbamem.2003.10.021.
104. Rostami, A.; Ciric, B. Role of Th17 cells in the pathogenesis of CNS inflammatory demyelination. *J. Neurol. Sci.* **2013**, *333*, 76–87, doi:10.1016/j.jns.2013.03.002.
105. Wagner, C.A.; Roqué, P.J.; Goverman, J.M. Pathogenic T cell cytokines in multiple sclerosis. *Journal of Experimental Medicine* **2020**, *217*, doi:10.1084/jem.20190460.
106. Ransohoff, R.M.; Estes, M.L. Astrocyte expression of major histocompatibility complex gene products in multiple sclerosis brain tissue obtained by stereotactic biopsy. *Arch. Neurol.* **1991**, *48*, 1244–1246, doi:10.1001/archneur.1991.00530240048017.
107. Zeinstra, E.; Wilczak, N.; Streefland, C.; Keyser, J. de. Astrocytes in chronic active multiple sclerosis plaques express MHC class II molecules. *Neuroreport* **2000**, *11*, 89–91, doi:10.1097/00001756-200001170-00018.
108. Zeinstra, E.; Wilczak, N.; Keyser, J. de. Reactive astrocytes in chronic active lesions of multiple sclerosis express co-stimulatory molecules B7-1 and B7-2. *Journal of Neuroimmunology* **2003**, *135*, 166–171, doi:10.1016/S0165-5728(02)00462-9.
109. Rostami, J.; Fotaki, G.; Sirois, J.; Mzezewa, R.; Bergström, J.; Essand, M.; Healy, L.; Erlandsson, A. Astrocytes have the capacity to act as antigen-presenting cells in the Parkinson's disease brain. *J. Neuroinflammation* **2020**, *17*, 119, doi:10.1186/s12974-020-01776-7.
110. Pagenstecher, A.; Lassmann, S.; Carson, M.J.; Kincaid, C.L.; Stalder, A.K.; Campbell, I.L. Astrocyte-targeted expression of IL-12 induces active cellular immune responses in the central nervous system and modulates experimental allergic encephalomyelitis. *J. Immunol.* **2000**, *164*, 4481–4492, doi:10.4049/jimmunol.164.9.4481.
111. Nitsch, L.; Petzinna, S.; Zimmermann, J.; Schneider, L.; Krauthausen, M.; Heneka, M.T.; Getts, D.R.; Becker, A.; Müller, M. Astrocyte-specific expression of interleukin 23 leads to an aggravated phenotype and enhanced inflammatory response with B cell accumulation in the EAE model. *J. Neuroinflammation* **2021**, *18*, 101, doi:10.1186/s12974-021-02140-z.
112. Sénécal, V.; Deblois, G.; Beauseigle, D.; Schneider, R.; Brandenburg, J.; Newcombe, J.; Moore, C.S.; Prat, A.; Antel, J.; Arbour, N. Production of IL-27 in multiple sclerosis lesions by astrocytes and myeloid cells: Modulation of local immune responses. *Glia* **2016**, *64*,

- 553–569, doi:10.1002/glia.22948.
113. Kim, R.Y.; Hoffman, A.S.; Itoh, N.; Ao, Y.; Spence, R.; Sofroniew, M.V.; Voskuhl, R.R. Astrocyte CCL2 sustains immune cell infiltration in chronic experimental autoimmune encephalomyelitis. *Journal of Neuroimmunology* **2014**, *274*, 53–61, doi:10.1016/j.jneuroim.2014.06.009.
114. Ponath, G.; Lincoln, M.R.; Levine-Ritterman, M.; Park, C.; Dahlawi, S.; Mubarak, M.; Sumida, T.; Airas, L.; Zhang, S.; Isitan, C.; et al. Enhanced astrocyte responses are driven by a genetic risk allele associated with multiple sclerosis. *Nat. Commun.* **2018**, *9*, 5337, doi:10.1038/s41467-018-07785-8.
115. Ambrosini, E.; Remoli, M.E.; Giacomini, E.; Rosicarelli, B.; Serafini, B.; Lande, R.; Aloisi, F.; Coccia, E.M. Astrocytes produce dendritic cell-attracting chemokines in vitro and in multiple sclerosis lesions. *J. Neuropathol. Exp. Neurol.* **2005**, *64*, 706–715, doi:10.1097/01.jnen.0000173893.01929.fc.
116. Grist, J.J.; Marro, B.S.; Skinner, D.D.; Syage, A.R.; Worne, C.; Doty, D.J.; Fujinami, R.S.; Lane, T.E. Induced CNS expression of CXCL1 augments neurologic disease in a murine model of multiple sclerosis via enhanced neutrophil recruitment. *Eur. J. Immunol.* **2018**, *48*, 1199–1210, doi:10.1002/eji.201747442.
117. Phares, T.W.; Stohlman, S.A.; Hinton, D.R.; Bergmann, C.C. Astrocyte-derived CXCL10 drives accumulation of antibody-secreting cells in the central nervous system during viral encephalomyelitis. *J. Virol.* **2013**, *87*, 3382–3392, doi:10.1128/JVI.03307-12.
118. Calderon, T.M.; Eugenin, E.A.; Lopez, L.; Kumar, S.S.; Hesselgesser, J.; Raine, C.S.; Berman, J.W. A role for CXCL12 (SDF-1alpha) in the pathogenesis of multiple sclerosis: regulation of CXCL12 expression in astrocytes by soluble myelin basic protein. *Journal of Neuroimmunology* **2006**, *177*, 27–39, doi:10.1016/j.jneuroim.2006.05.003.
119. Maier, J.; Kincaid, C.; Pagenstecher, A.; Campbell, I.L. Regulation of Signal Transducer and Activator of Transcription and Suppressor of Cytokine-Signaling Gene Expression in the Brain of Mice with Astrocyte-Targeted Production of Interleukin-12 or Experimental Autoimmune Encephalomyelitis. *Am. J. Pathol.* **2002**, *160*, 271–288, doi:10.1016/S0002-9440(10)64371-4.
120. Yu, S.; Jia, L.; Zhang, Y.; Zhong, J.; Yang, B.; Wu, C. IL-12 induced the generation of IL-21- and IFN- $\gamma$ -co-expressing poly-functional CD4<sup>+</sup> T cells from human naive CD4<sup>+</sup> T cells. *Cell Cycle* **2015**, *14*, 3362–3372, doi:10.1080/15384101.2015.1093703.
121. Beurel, E.; Harrington, L.E.; Buchser, W.; Lemmon, V.; Jope, R.S. Astrocytes modulate the polarization of CD4<sup>+</sup> T cells to Th1 cells. *PLoS One* **2014**, *9*, e86257, doi:10.1371/journal.pone.0086257.
122. Fletcher, J.M.; Lalor, S.J.; Sweeney, C.M.; Tubridy, N.; Mills, K.H.G. T cells in multiple sclerosis and experimental autoimmune encephalomyelitis. *Clin. Exp. Immunol.* **2010**, *162*, 1–11, doi:10.1111/j.1365-2249.2010.04143.x.
123. Constantinescu, C.S.; Tani, M.; Ransohoff, R.M.; Wysocka, M.; Hilliard, B.; Fujioka, T.; Murphy, S.; Tighe, P.J.; Das Sarma, J.; Trinchieri, G.; et al. Astrocytes as antigen-presenting cells: expression of IL-12/IL-23. *J. Neurochem.* **2005**, *95*, 331–340, doi:10.1111/j.1471-4159.2005.03368.x.
124. Thakker, P.; Leach, M.W.; Kuang, W.; Benoit, S.E.; Leonard, J.P.; Marusic, S. IL-23 is critical in the induction but not in the effector phase of experimental autoimmune



- encephalomyelitis. *J. Immunol.* **2007**, *178*, 2589–2598, doi:10.4049/jimmunol.178.4.2589.
125. Harrington, L.E.; Hatton, R.D.; Mangan, P.R.; Turner, H.; Murphy, T.L.; Murphy, K.M.; Weaver, C.T. Interleukin 17-producing CD4+ effector T cells develop via a lineage distinct from the T helper type 1 and 2 lineages. *Nat. Immunol.* **2005**, *6*, 1123–1132, doi:10.1038/ni1254.
126. Veldhoen, M.; Hocking, R.J.; Atkins, C.J.; Locksley, R.M.; Stockinger, B. TGF $\beta$  in the Context of an Inflammatory Cytokine Milieu Supports De Novo Differentiation of IL-17-Producing T Cells. *Immunity* **2006**, *24*, 179–189, doi:10.1016/j.immuni.2006.01.001.
127. Kim, D.; Le, H.T.; Nguyen, Q.T.; Kim, S.; Lee, J.; Min, B. Cutting Edge: IL-27 Attenuates Autoimmune Neuroinflammation via Regulatory T Cell/Lag3-Dependent but IL-10-Independent Mechanisms In Vivo. *J. Immunol.* **2019**, *202*, 1680–1685, doi:10.4049/jimmunol.1800898.
128. Murugaiyan, G.; Mittal, A.; Lopez-Diego, R.; Maier, L.M.; Anderson, D.E.; Weiner, H.L. IL-27 is a key regulator of IL-10 and IL-17 production by human CD4+ T cells. *J. Immunol.* **2009**, *183*, 2435–2443, doi:10.4049/jimmunol.0900568.
129. Gschwandtner, M.; Derler, R.; Midwood, K.S. More Than Just Attractive: How CCL2 Influences Myeloid Cell Behavior Beyond Chemotaxis. *Front. Immunol.* **2019**, *10*, 2759, doi:10.3389/fimmu.2019.02759.
130. Prins, M.; Dutta, R.; Baselmans, B.; Brevé, J.J.P.; Bol, J.G.J.M.; Deckard, S.A.; van der Valk, P.; Amor, S.; Trapp, B.D.; Vries, H.E. de; et al. Discrepancy in CCL2 and CCR2 expression in white versus grey matter hippocampal lesions of Multiple Sclerosis patients. *Acta Neuropathol. Commun.* **2014**, *2*, 98, doi:10.1186/s40478-014-0098-6.
131. Moreno, M.; Bannerman, P.; Ma, J.; Guo, F.; Miers, L.; Soulika, A.M.; Pleasure, D. Conditional ablation of astroglial CCL2 suppresses CNS accumulation of M1 macrophages and preserves axons in mice with MOG peptide EAE. *J. Neurosci.* **2014**, *34*, 8175–8185, doi:10.1523/JNEUROSCI.1137-14.2014.
132. He, M.; Dong, H.; Huang, Y.; Lu, S.; Zhang, S.; Qian, Y.; Jin, W. Astrocyte-Derived CCL2 is Associated with M1 Activation and Recruitment of Cultured Microglial Cells. *Cell. Physiol. Biochem.* **2016**, *38*, 859–870, doi:10.1159/000443040.
133. Marques, R.E.; Guabiraba, R.; Russo, R.C.; Teixeira, M.M. Targeting CCL5 in inflammation. *Expert Opin. Ther. Targets* **2013**, *17*, 1439–1460, doi:10.1517/14728222.2013.837886.
134. Szczuciński, A.; Losy, J. CCL5, CXCL10 and CXCL11 chemokines in patients with active and stable relapsing-remitting multiple sclerosis. *Neuroimmunomodulation* **2011**, *18*, 67–72, doi:10.1159/000317394.
135. dos Santos, A.C.; Barsante, M.M.; Arantes, R.M.E.; Bernard, C.C.A.; Teixeira, M.M.; Carvalho-Tavares, J. CCL2 and CCL5 mediate leukocyte adhesion in experimental autoimmune encephalomyelitis--an intravital microscopy study. *Journal of Neuroimmunology* **2005**, *162*, 122–129, doi:10.1016/j.jneuroim.2005.01.020.
136. Ranasinghe, R.; Eri, R. CCR6–CCL20 Axis in IBD: What Have We Learnt in the Last 20 Years? *GastrointestDisord* **2018**, *1*, 57–74, doi:10.3390/gidisord1010006.
137. Ambrosini, E.; Columba-Cabezas, S.; Serafini, B.; Muscella, A.; Aloisi, F. Astrocytes are the major intracerebral source of macrophage inflammatory protein-3 $\alpha$ /CCL20 in relapsing experimental autoimmune encephalomyelitis and in vitro. *Glia* **2003**, *41*, 290–

- 300, doi:10.1002/glia.10193.
138. Li, R.; Sun, X.; Shu, Y.; Wang, Y.; Xiao, L.; Wang, Z.; Hu, X.; Kermode, A.G.; Qiu, W. Serum CCL20 and its association with SIRT1 activity in multiple sclerosis patients. *Journal of Neuroimmunology* **2017**, *313*, 56–60, doi:10.1016/j.jneuroim.2017.10.013.
  139. Huang, J.; Khademi, M.; Fugger, L.; Lindhe, Ö.; Novakova, L.; Axelsson, M.; Malmeström, C.; Constantinescu, C.; Lycke, J.; Piehl, F.; et al. Inflammation-related plasma and CSF biomarkers for multiple sclerosis. *Proc. Natl. Acad. Sci. U.S.A.* **2020**, *117*, 12952–12960, doi:10.1073/pnas.1912839117.
  140. Reboldi, A.; Coisne, C.; Baumjohann, D.; Benvenuto, F.; Bottinelli, D.; Lira, S.; Uccelli, A.; Lanzavecchia, A.; Engelhardt, B.; Sallusto, F. C-C chemokine receptor 6-regulated entry of TH-17 cells into the CNS through the choroid plexus is required for the initiation of EAE. *Nat. Immunol.* **2009**, *10*, 514–523, doi:10.1038/ni.1716.
  141. Omari, K.M.; John, G.; Lango, R.; Raine, C.S. Role for CXCR2 and CXCL1 on glia in multiple sclerosis. *Glia* **2006**, *53*, 24–31, doi:10.1002/glia.20246.
  142. Filipovic, R.; Zecevic, N. The effect of CXCL1 on human fetal oligodendrocyte progenitor cells. *Glia* **2008**, *56*, 1–15, doi:10.1002/glia.20582.
  143. Tsai, H.-H.; Frost, E.; To, V.; Robinson, S.; French-Constant, C.; Geertman, R.; Ransohoff, R.M.; Miller, R.H. The Chemokine Receptor CXCR2 Controls Positioning of Oligodendrocyte Precursors in Developing Spinal Cord by Arresting Their Migration. *Cell* **2002**, *110*, 373–383, doi:10.1016/S0092-8674(02)00838-3.
  144. Omari, K.M.; Lutz, S.E.; Santambrogio, L.; Lira, S.A.; Raine, C.S. Neuroprotection and remyelination after autoimmune demyelination in mice that inducibly overexpress CXCL1. *Am. J. Pathol.* **2009**, *174*, 164–176, doi:10.2353/ajpath.2009.080350.
  145. Sørensen, T.L.; Trebst, C.; Kivisäkk, P.; Klaege, K.L.; Majmudar, A.; Ravid, R.; Lassmann, H.; Olsen, D.B.; Strieter, R.M.; Ransohoff, R.M.; et al. Multiple sclerosis: a study of CXCL10 and CXCR3 co-localization in the inflamed central nervous system. *Journal of Neuroimmunology* **2002**, *127*, 59–68, doi:10.1016/S0165-5728(02)00097-8.
  146. Mills Ko, E.; Ma, J.H.; Guo, F.; Miers, L.; Lee, E.; Bannerman, P.; Burns, T.; Ko, D.; Sohn, J.; Soulika, A.M.; et al. Deletion of astroglial CXCL10 delays clinical onset but does not affect progressive axon loss in a murine autoimmune multiple sclerosis model. *J. Neuroinflammation* **2014**, *11*, 105, doi:10.1186/1742-2094-11-105.
  147. Boztug, K.; Carson, M.J.; Pham-Mitchell, N.; Asensio, V.C.; DeMartino, J.; Campbell, I.L. Leukocyte infiltration, but not neurodegeneration, in the CNS of transgenic mice with astrocyte production of the CXC chemokine ligand 10. *J. Immunol.* **2002**, *169*, 1505–1515, doi:10.4049/jimmunol.169.3.1505.
  148. Marastoni, D.; Magliozzi, R.; Bolzan, A.; Pisani, A.I.; Rossi, S.; Crescenzo, F.; Montemezzi, S.; Pizzini, F.B.; Calabrese, M. CSF Levels of CXCL12 and Osteopontin as Early Markers of Primary Progressive Multiple Sclerosis. *Neurol. Neuroimmunol. Neuroinflamm.* **2021**, *8*, doi:10.1212/NXI.0000000000001083.
  149. Krumbholz, M.; Theil, D.; Cepok, S.; Hemmer, B.; Kivisäkk, P.; Ransohoff, R.M.; Hofbauer, M.; Farina, C.; Derfuss, T.; Hartle, C.; et al. Chemokines in multiple sclerosis: CXCL12 and CXCL13 up-regulation is differentially linked to CNS immune cell recruitment. *Brain* **2006**, *129*, 200–211, doi:10.1093/brain/awh680.
  150. Zilkha-Falb, R.; Kaushansky, N.; Kawakami, N.; Ben-Nun, A. Post-CNS-inflammation

- expression of CXCL12 promotes the endogenous myelin/neuronal repair capacity following spontaneous recovery from multiple sclerosis-like disease. *J. Neuroinflammation* **2016**, *13*, 7, doi:10.1186/s12974-015-0468-4.
151. Patel, J.R.; McCandless, E.E.; Dorsey, D.; Klein, R.S. CXCR4 promotes differentiation of oligodendrocyte progenitors and remyelination. *Proc. Natl. Acad. Sci. U.S.A.* **2010**, *107*, 11062–11067, doi:10.1073/pnas.1006301107.
  152. Meiron, M.; Zohar, Y.; Anunu, R.; Wildbaum, G.; Karin, N. CXCL12 (SDF-1 $\alpha$ ) suppresses ongoing experimental autoimmune encephalomyelitis by selecting antigen-specific regulatory T cells. *Journal of Experimental Medicine* **2008**, *205*, 2643–2655, doi:10.1084/jem.20080730.
  153. McCandless, E.E.; Wang, Q.; Woerner, B.M.; Harper, J.M.; Klein, R.S. CXCL12 limits inflammation by localizing mononuclear infiltrates to the perivascular space during experimental autoimmune encephalomyelitis. *J. Immunol.* **2006**, *177*, 8053–8064, doi:10.4049/jimmunol.177.11.8053.
  154. Kipp, M.; Clarner, T.; Gingele, S.; Pott, F.; Amor, S.; van der Valk, P.; Beyer, C. Brain lipid binding protein (FABP7) as modulator of astrocyte function. *Physiol. Res.* **2011**, *60*, S49–60, doi:10.33549/physiolres.932168.
  155. Brosnan, C.F.; Raine, C.S. The astrocyte in multiple sclerosis revisited. *Glia* **2013**, *61*, 453–465, doi:10.1002/glia.22443.
  156. Ludwin, S.K.; Rao, V.T.; Moore, C.S.; Antel, J.P. Astrocytes in multiple sclerosis. *Mult. Scler.* **2016**, *22*, 1114–1124, doi:10.1177/1352458516643396.
  157. Lassmann, H. Multiple Sclerosis Pathology. *Cold Spring Harb. Perspect. Med.* **2018**, *8*, doi:10.1101/cshperspect.a028936.
  158. Ridet, J.L.; Privat, A.; Malhotra, S.K.; Gage, F.H. Reactive astrocytes: cellular and molecular cues to biological function. *Trends Neurosci.* **1997**, *20*, 570–577, doi:10.1016/S0166-2236(97)01139-9.
  159. Lau, L.W.; Keough, M.B.; Haylock-Jacobs, S.; Cua, R.; Döring, A.; Sloka, S.; Stirling, D.P.; Rivest, S.; Yong, V.W. Chondroitin sulfate proteoglycans in demyelinated lesions impair remyelination. *Ann. Neurol.* **2012**, *72*, 419–432, doi:10.1002/ana.23599.
  160. Stephenson, E.L.; Mishra, M.K.; Moussienko, D.; Laflamme, N.; Rivest, S.; Ling, C.-C.; Yong, V.W. Chondroitin sulfate proteoglycans as novel drivers of leucocyte infiltration in multiple sclerosis. *Brain* **2018**, *141*, 1094–1110, doi:10.1093/brain/awy033.
  161. Haindl, M.T.; Köck, U.; Zeitelhofer-Adzemovic, M.; Fazekas, F.; Hochmeister, S. The formation of a glial scar does not prohibit remyelination in an animal model of multiple sclerosis. *Glia* **2019**, *67*, 467–481, doi:10.1002/glia.23556.
  162. Yang, Z.; Wang, K.K.W. Glial fibrillary acidic protein: from intermediate filament assembly and gliosis to neurobiomarker. *Trends Neurosci.* **2015**, *38*, 364–374, doi:10.1016/j.tins.2015.04.003.
  163. Liddel, S.A.; Barres, B.A. Reactive Astrocytes: Production, Function, and Therapeutic Potential. *Immunity* **2017**, *46*, 957–967, doi:10.1016/j.immuni.2017.06.006.
  164. Cordiglieri, C.; Farina, C. Astrocytes Exert and Control Immune Responses in the Brain. *CIR* **2010**, *6*, 150–159, doi:10.2174/157339510791823655.
  165. Krupenko, N.I.; Sharma, J.; Fogle, H.M.; Padiaditakis, P.; Strickland, K.C.; Du, X.; Helke, K.L.; Sumner, S.; Krupenko, S.A. Knockout of Putative Tumor Suppressor Aldh111 in Mice

- Reprograms Metabolism to Accelerate Growth of Tumors in a Diethylnitrosamine (DEN) Model of Liver Carcinogenesis. *Cancers (Basel)* **2021**, *13*, doi:10.3390/cancers13133219.
166. Chen, X.-Q.; He, J.-R.; Wang, H.-Y. Decreased expression of ALDH1L1 is associated with a poor prognosis in hepatocellular carcinoma. *Med. Oncol.* **2012**, *29*, 1843–1849, doi:10.1007/s12032-011-0075-x.
167. Garcia-Esparcia, P.; Diaz-Lucena, D.; Ainciburu, M.; Torrejón-Escribano, B.; Carmona, M.; Llorens, F.; Ferrer, I. Glutamate Transporter GLT1 Expression in Alzheimer Disease and Dementia With Lewy Bodies. *Front. Aging Neurosci.* **2018**, *10*, 122, doi:10.3389/fnagi.2018.00122.
168. Castillo-Rodriguez, M.d.L.A.; Gingele, S.; Schröder, L.-J.; Möllenkamp, T.; Stangel, M.; Skripuletz, T.; Gudi, V. Astroglial and oligodendroglial markers in the cuprizone animal model for de- and remyelination. *Histochem. Cell Biol.* **2022**, doi:10.1007/s00418-022-02096-y.
169. Williams, S.R.; Yang, Q.; Chen, F.; Liu, X.; Keene, K.L.; Jacques, P.; Chen, W.-M.; Weinstein, G.; Hsu, F.-C.; Beiser, A.; et al. Genome-wide meta-analysis of homocysteine and methionine metabolism identifies five one carbon metabolism loci and a novel association of ALDH1L1 with ischemic stroke. *PLoS Genet.* **2014**, *10*, e1004214, doi:10.1371/journal.pgen.1004214.

# 11. Appendix

## 11.1 Chemicals

Table 13: List of chemicals

Chemical	Supplier	Order number
Citric acid monohydrate	Carl Roth, Germany	1818.1
Cuprizone	Sigma Aldrich, Germany	C9012
DAPI	Roth, Germany	6335.1
DePex	Serva	18243.02
EDTA	Roth, Germany	X986.2
Elite ABC HRP Kit	Vector Laboratories, USA	PK-6101
Ethanol 96%	Walter CMP, Germany	WAL641 6025
Ethanol 100%	Walter CMP, Germany	WAL642 6025
Formaldehyde 37%	Merck, Germany	1.03999.1000
HCL 37%	Merck, Germany	1.00317.1000
Hematoxylin	Sigma Aldrich, Germany	1092490500
H <sub>2</sub> O <sub>2</sub> 35%	Roth, Germany	8070.4
Ketamine	bela-pharm, Germany	Zul.-Nr. 9089.01.00
Liquid DAB+ Substrate Chromogen System	Agilent Technologies, USA	K3468
NaH <sub>2</sub> PO <sub>4</sub>	Merck, Germany	1.06346.1000,
Na <sub>2</sub> HPO <sub>4</sub>	Merck, Germany	1.06580.1000
sodium chloride (NaCl)	Roth, Germany	0962.2
NaOH	Merck, Germany	1.06469.1000
Normal donkey Serum	Abcam, UK	ab7475
Normal goat serum	Vector Laboratories, USA	S-1000
Paraffin	Merck, Germany	1.07158.9025
potassium chloride (KCl)	Roth, Germany	6781.2
Potassium dihydrogen phosphate (KH <sub>2</sub> PO <sub>4</sub> )	Roth, Germany	P018.2
TRIS	Roth, Germany	AE15.2
Xylazine	Bayer, Germany	Zul.-Nr. 6293841.00.00
Xylene	J.T.Baker, USA	8118

## 11.2 Solutions

Table 14: List of solutions

Solution	Recipe
ABC-HRP system	2% v/v Reagent A 2% v/v Reagent B 96% v/v PBS
serum Blocking solution	5% v/v normal serum (goat or donkey) 95% v/v PBS
Citrate buffer (PH 6.0)	2.3g/L Citric acid monohydrate Distilled water
DAB solution	98% v/v DAB substrate buffer 2% v/v DAB chromogen
PBS (PH 7.4)	8.0g/L NaCl 0.2/L KCl 1.68g/L Na <sub>2</sub> HPO <sub>4</sub> 0.27g/L KH <sub>2</sub> PO <sub>4</sub> Distilled water
TRIS/EDTA buffer (PH 9.0)	1.21g/L Tris 0.37g/L EDTA Distilled water

## 12. Personal declaration

I hereby declare that this thesis with the title “astrocytic expression of aldehyde dehydrogenase family 1 member L1” is the result of my work under the instruction of Uni. Prof. Dr. med. Dr. rer. nat. Markus Kipp. This dissertation has not been submitted to other institutions for benefits of a degree, diploma. Sources from others directly or reprocessed have been indicated.

Rostock, 11.07.2022

Feifei Liu

## 13. Acknowledgements

During my study in Germany for 2 years, I have received a great deal of invaluable help from others.

I would like to say sincere thanks to my supervisor, Professor Markus Kipp, whose professional guidance and feedback helped me complete this project. I owe many thanks to technicians because their supports really solved lots of technical problems I met. I am grateful to my colleagues who really aided me substantially when I processed the data and images.

It is a great honor for me to study with so many talented people in Rostock and live in such a city with picturesque scenery. It is an unforgettable experience for me.

Feifei Liu



## 14. Curriculum Vitae

Surname and first name: Feifei Liu

Date Of Birth: 23.09.1985, Nationality: China

Research experience:

MD student, University of Rostock, Germany, August 2020 – May 2022

Master student, Wuhan University, China, August 2009 – June 2012

Publications:

Liu Feifei, Sarah Joost, Markus Kipp: Spontaneous hind limb paralysis due to acute precursor B cell leukemia in RAG1-deficient mice. Journal of Molecular Neuroscience, 18 May 2022.

Feifei Liu